CHAPTER 2

IONOSPHERIC EFFECTS

2.1 PROPAGATION IN HOMOGENEOUS PLASMAS

This chapter includes a brief treatment of ionospheric propagation. The reader interested in a more thorough analysis of this large and interesting subject is referred to treatises by Budden (1951), Davies (1965, 1969), Kelso (1964), and Ratcliffe (1972). An elementary introduction starting with Maxwell's equations was given by Flock (1979)0

2.1.1 Characteristic Waves

The Earth's ionosphere is a partially ionized gas or plasma which is rendered anisotropic by the presence of the Earth's magnetic field. The concept of characteristic waves is important in considering the propagation of electromagnetic waves in such a medium. These are the waves which propagate without changing their polarization, by which reference is made to whether a wave is linearly, circularly, or elliptically polarized and, in the case of linear polarization, to the direction of the electric field intensity vector of the wave (e.g. vertical, horizontal, or at an angle between vertical and horizontal). Changing from right circular to left circular polarization, for example, constitutes a change in polarization, and changing the direction of linear polarization also constitutes a change in polarization.

The nature of the characteristic waves that propagate in an anisotropic plasma such as the Earth's ionosphere canbe determined by the application of Maxwell's equations. It develops that there are two characteristic waves and that the parameters of the characteristic waves depend upon the direction of propagation with respect to the Earth's magnetic field (the angle θ_B of Fig. 2.1).

Parallel Propagation

For propagation parallel to the Earth's field B ($\theta_B = 0^o$) in the lossless case the two characteristic waves are left and right circularly polarized and have indices of refraction n_l and nrgiven by

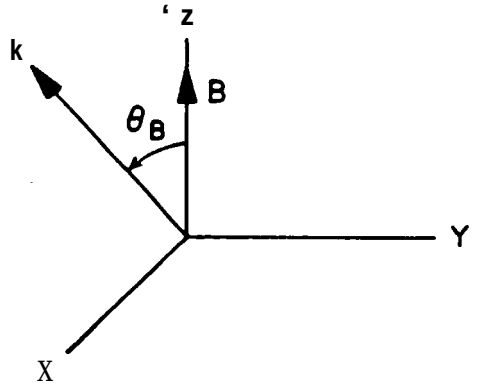

Figure 2.1 'Coordinate system for considering propagation at an angle θ_B from the direction of the Earth's field B.

$$n_l^2 = K_l = 1 - \frac{\omega_p^2}{\omega(\omega + \omega_B)} \qquad (2.1)$$

and

$$n_r^2 = K_r = 1 - \frac{\omega_p^2}{\omega(\omega - \omega_B)} \qquad (2.2)$$

K_l and K_r are the relative dielectric constants for the left and right circularly polarized waves. The quantity ω is the angular frequency of the wave and equals $2\pi f$ where f is frequency in Hz, while ω_B is the angular gyrofrequency of the electrons in the plasma and is given by

$$\omega_B \quad \frac{-qB}{m} \qquad (2.3)$$

where B is the Earth's magnetic field in Wb/m^2. q = -e = -1.6022 x 10^{-19} C is the charge of the electron, and m is the mass of the electron (9. 1096 x 10^{-31} kg). The Earth's field is roughly that of

a magnetic dipole, inclined by about 12 deg with respect to the rotational axis, for which the field decreases as the cube of the radius or distance from the center of the Earth. Figure 2.2 shows field values given by a dipole model. For a more accurate model, reference can be made to the International Geomagnetic Reference Field (IGRF) developed by a working group of IAGA (The International Association of Geomagnetism and Aeronomy). A special issue of the Journal of Geomagnetism and Geoelectricity was devoted to the third-generation IGRF model (vol. 34, No. 6, pp. 307-422, 1982), and Appendix 2.2 describes briefly the basis for the IGRF models. A paper by Peddie (1982) in vol. 34 describes the third-generation 1980 model and also the IGRF 1965 and 1975 first- and second-generation models. All of the models include extrapolation ahead, and the third-generation model for 1980 includes extrapolation to 1985. The 1985 or fourth-generation IGRF model was presented in the June 17, 1986 issue of EOS. Numerical values of the 1985 coefficients of the spherical harmonic expansion of the geomagnetic field (Appendix 2.2) are included in this article in EOS.

A description of a computer algorithm for synthesizing the geomagnetic field from values of the spherical harmonic coefficients is given in a paper by Malin and Barraclough (1981). The coefficients of the IGRF models and computer programs for synthesizing field values are also available in the United States from the following sources.

World Data Center A, NOAA
NESDIS/NGDC (E/GC11)
325 Broadway, Boulder, CO 80303

World Data Center A for Rockets and Satellites
Code 601, NASA/Goddard Space Flight Center
Greenbelt, MD 20771

The geomagnetic models archived at the National Geophysical Data Center (NGDC) of NOAA in Boulder are described in a leaflet, Magnetic Field Models, updated in January 1986 and available from the center. Several models in addition to IGRF models are

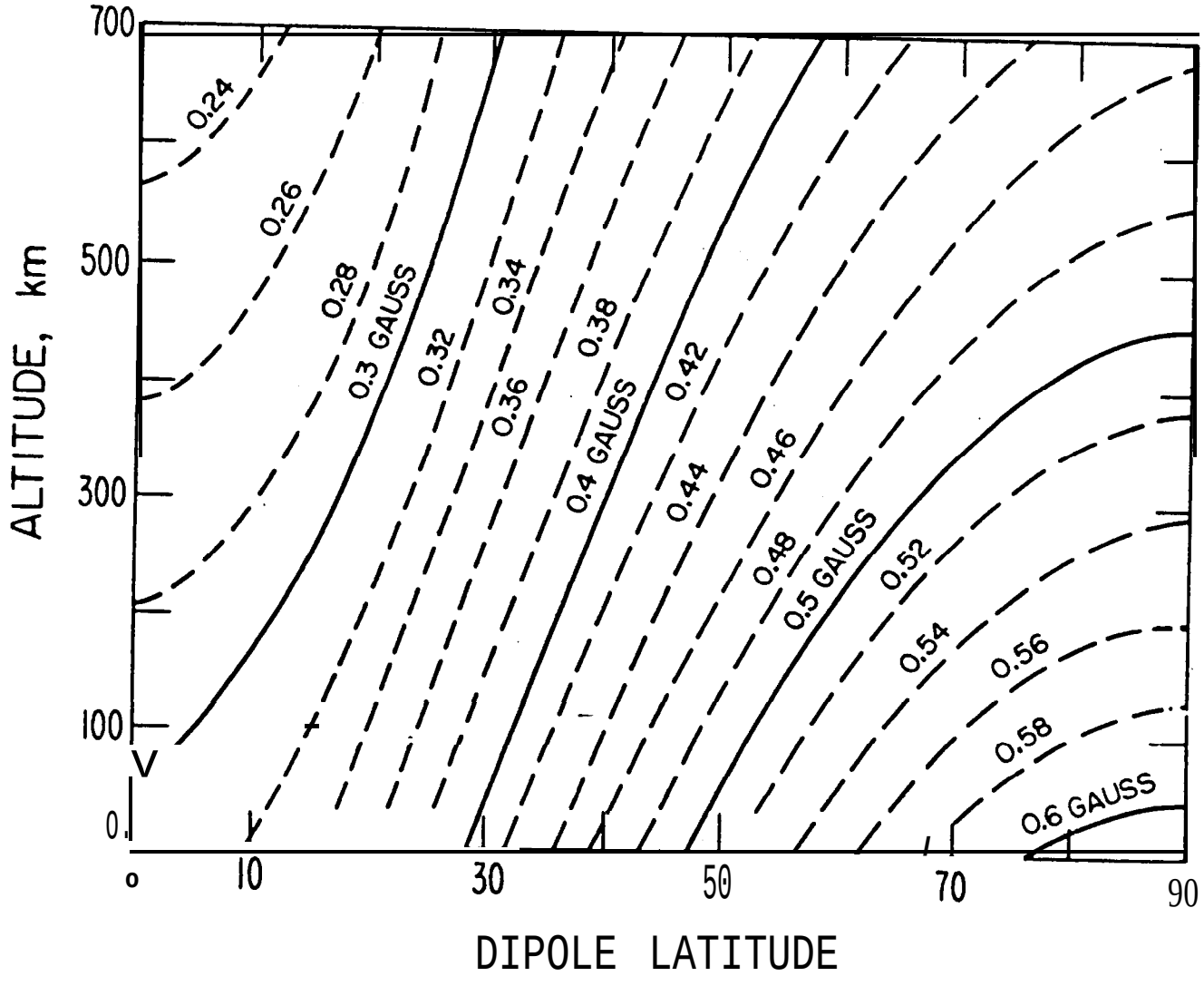

Figure 2.2 Total intensity of the Earth's magnetic field as a function of altitude and dipole latitude, assuming an earth-centered dipole of magnetic moment M = 7.95 x 10^{25} gauss cm^3 (after Smith, 1974).

archived, and, although we referred above to the 1965 model as the first generation IGRF model, the leaflet refers to the IGRF as involving earlier models as well.

The quantity ω^2 is the angular plasma frequency squared and can be found by using [p]

$$\omega_p^2 = Nq^2/(m\epsilon_o) \tag{2.4}$$

where N is electron density (el/m^3) and ϵ_o is the electric permittivity of empty space (8.854 x 10^{-12} F/m), For practical applications it may be convenient to convert from angular frequency to frequency in MHz for propagation at HF and higher frequencies. To this end

$$(fB)_{MHz} = 2.7992 \times 10^4 B \simeq 2.8 \times 10^4 B \tag{2.5}$$

with B in Wb/m^2, or $(fB)MH_z \simeq 2.8$ B with B in gauss. A. so

$$(f_p)_{MHz} = 8.9788 \times 10^{-6} N^{1/2} \tag{2.6}$$

with N the number of electrons per m^3. Then

$$n_l = \left[1 - \frac{f_p^2}{f\,(f + f_B)} \right]^{1/2} \tag{2.7}$$

$$n_r = \left[1 - \frac{f_p^2}{f\,(f - fB)} \right]^{1/2} \tag{2.8}$$

Perpendicular Propagation

For propagation perpendicular to the magnetic field (θ_B = 90 deg) one characteristic wave has its electric field intensity vector directed along the z axis of Fig. 2.1. The index of refraction no and relative dielectric constant K. in this case are given by

$$n_o^2 = K_o = 1 - \omega_p^2/\omega^2 = 1 - f_p^2/f^2 \tag{2.9}$$

which also apply for the case of no magnetic field. The subscript o stands for ordinary; the ordinary wave is unaffected by the magnetic field for perpendicular or transverse propagation. If the electric field intensity is in the y direction in Fig. 2.1 (or in general perpendicular to B), the situation is somewhat more complicated. In this case, the index of refraction n_x and the relative dielectric constant K_x are given by

$$n_x^2 = K_x = K_1 K_r / K_\perp \qquad (2.10)$$

where

$$K_1 = 1 - \frac{\omega_p^2}{\omega^2 - \omega_p^2}$$

This wave is referred to as the extraordinary wave. The two characteristic waves for propagation perpendicular or transerve to the magnetic field are linearly polarized in the plane perpendicular to the direction of propagation, but it develops that for the extraordinary wave there is a component of electric field intensity in the direction of propagation (the x direction if the transverse component is in the y direction).

2.1.2 Role of Index of Refraction

The index of refraction n of an electromagnetic wave is by definition the ratio of $c \simeq 2.9979 \times 10^8$ m/s, the velocity of an electromagnetic wave in empty space, to v_p, the velocity of the wave in question in the medium. Thus

$$n = c/v_p \qquad (2.11)$$

The phase constant β of an electromagnetic wave gives the phase lag of the wave with distance when used in

$$E = E_o e^{-j\beta z} \qquad (2.12)$$

for the case of a wave propagating in the z direction and having an electric field intensity E_o at a reference position where z = O. The constant β can be expressed in several ways as shown by Eq. (2. 13).

$$\beta = 2\pi/\lambda = \omega/v_p = \beta_o n \qquad (2.13)$$

where λ is wavelength and β_o is the phase constant of empty space. It was shown earlier that the two characteristic waves, for propagation either parallel or perpendicular to the magnetic field, have different values of index of refraction. Thus they have different phase velocities, phase constants, and wavelengths.

2.1.3 Reflection and Refraction

Reflection

Examination of the expressions for relative dielectric constant, Eq. (2.9) for the ordinary wave for transverse propagation for example, reveals that it is possible for the dielectric constant to be negative and that the index of refraction can thus become imaginary. For $\omega > \omega_p$ in Eq. (2.9) no is real, but, for $\omega < \omega_p$, no is imaginary. 'An imaginary value of index of refraction determines that β of Eq. (2. 12) will also be imaginary so that, instead of a propagating wave as indicated in Eq. (2. 12), an evanescent condition will occur so that $E = E_o e^{-\alpha z}$ because the quantity $-j\beta$ of Eq. (2. 12) has become $-j\beta_o\ (-j|n|) = -\alpha$. The different possibilities are summarized in Table 2.1.

Table 2.1 Characteristics of n and E(z) Corresponding to Different Relative Values of ω and ω_p.

ω	n	E(z)
$\omega > \omega_p$	real	$E = E_o e^{-j\beta z}$
$\omega = \omega_p$	o	$E = E_o$
$\omega < \omega_p$	- imaginary	$E = E_o e^{-\alpha z}$

The, condition $E = E_o e^{-\alpha z}$ of Table 2.1 represents a field that attenuates with z, but the attenuation in this case is not dissipative. Instead it involves reflection and reversal of directional sug_ested in Fig. 2. 3b. In Fig. 2.3 an increase of electron density with_eight in the ionosphere is assumed. The frequency ω is much greater than ω_p in Fig. 2.3a, and the ray path is essential y unaffected by the ionosphere, whether the pathis vertical or oblique. In Fig. 2.3b the condition $\omega < \omega_p$ is reached in the vertical path shown and the ray is reflected. Figure 2.3b suggests the overall result, but the

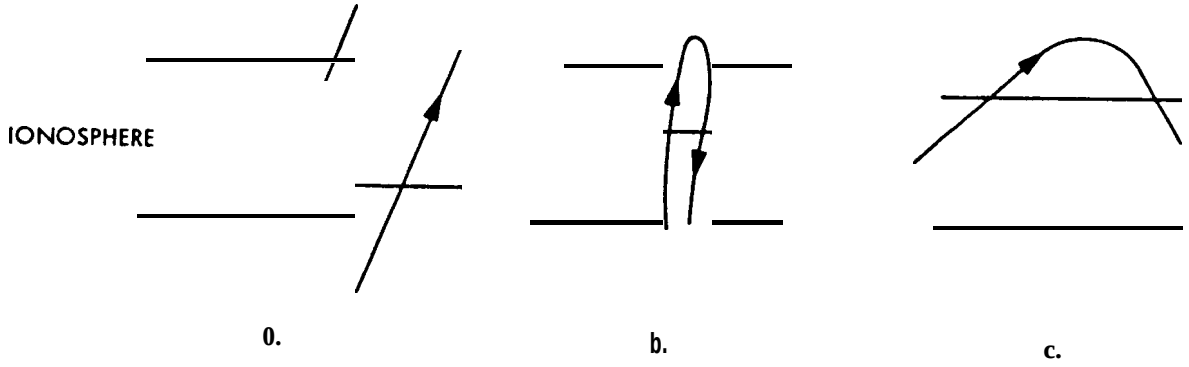

Figure 2.3 Ionospheric ray paths.

a. $\omega >> \omega_p$ throughout.

b. The condition $\omega < \omega_p$ is reached along the ray path,

c. Oblique-incidence path.

reflection process actually takes place over a range of heights, consistent with $E = E_o e^{-\alpha z}$, rather than abruptly at a particular level. Furthermore, if the evanscent region is of limited extent and E still has a significant value at the far side of the region from the source, then a wave of diminished amplitude will be launched and will propagate beyond the evanscent region.

For the ordinary wave ω_p plays the role of a critical frequency with propagation occurring for $\omega > \omega_p$ and not for $\omega < \omega_p$. The situation is similar to propa gtion in a metallic waveguide having a certain cutoff frequency f_c. Ina waveguide propagation occurs for $f > f_c$ and an evanescent condition occurs for $f < f_c$. An evanescent section of waveguide can serve as a waveguide-below-cutoff attenuator. For the left and right circularly polarized waves, Eqs. (2. i) and (2.2) show that the conditions $\omega_p^2 = \omega^2 + \omega\omega_B$ and $\omega_p^2 = \omega^2 - \omega\omega_B$ separate propagating and nonpropagating regions for the left and right circularly polarized waves, respectively.

The above discussion is idealized in that dissipative attenuation does occur to some degree in the ionosphere so that, for $\omega > \omega_p$, $E(z) = E_o e^{-j\beta z} e^{-\alpha z}$ where now α represents dissipative attenuation involving the conversion of electromagnetic energy into heat, The topic of absorption or dissipative attenuation is treated in Sec. 2.7.

Refraction

In Fig. 2.3c a ray is obliquely incident upon the ionosphere and is shown to experience reflection, In this case ω is always greater than ω_p, however, and while the overall result is usually viewed as reflection the process is basically one of refraction. Applying Snell's law with the angle χ measured from the zenith and neglecting the Earth's curvature, $n \sin \chi = n_o \sin \chi_o$ where χ_o is the initial launch angle below the ionosphere and n_o, the index of refraction of the troposphere, is essentially unity. At the highest point in the path of Fig. 2.3c the angle χ is 90 deg. Therefore, at this point $n = \sin \chi_o$. For the ordinary wave and transverse propagation

$$n^2 = 1 - (f_p/f)^2$$

with f_p the plasma frequency and f the operating frequency. Therefore

$$n^2 = \sin^2 \chi_o = 1 - (f_p/f)^2 \qquad (2.14)$$

from which $\cos \chi_0 = f_p / f$ and

$$f = f_p \sec \chi_o \qquad (2.15)$$

This expression gives the maximum frequency, f, which will be reflected, or refracted, from or below a height where the plasma frequency is f_p in the case of a wave having a launch angle of χ_o. If f_p is the peak plasma frequency in the ionosphere then f is the maximum usable frequency, in particular the maximum frequency that will be reflected for a launch angle of χ_o.

The above case can be considered to be an extreme example of refraction. At the frequencies of major interest in this handbook, ionospheric refraction will be of rather minor importance but will cause a slight bending of a ray such that the apparent elevation angle of arrival will be higher than the geometric elevation angle. For satellites well above most of the ionization the error in elevation angle $\Delta\theta$ is given by

$$\Delta\theta = \frac{(R + r. \sin \theta_o) \, r \cos \theta_0}{[h_i(2r_o + hi) + (r_o \sin 0.)^2]} \frac{\Delta R}{R} \quad \text{rad} \qquad (2.16)$$

where θ_o is the apparent elevation angle, hi is the height of the centroid of the electron content along the path (normally between 300 and 450 km), and AR is the range error [Eq. (2.3'4)]. For sufficiently low elevation angles or for long ranges corresponding to geostationary satellites for which R) r. sin 9_0

$$\Delta\theta \simeq \frac{\cos e_o}{2 h_i} AR \quad \text{rad} \qquad (2.17)$$

As AR, the range error, varies with time, the elevation angle error $\Delta\theta$ also varies with time. Furthermore as $\Delta\theta$ is the difference between the true and apparent elevation angles, the apparent elevation angle or direction of arrival varies with time,

These relations were developed by Millman and Reinsmith (1974). Klobuchar (1 978) reports that for a frequency of 1.6 GHz, a worst case elevation angle of 5 deg, and a TEC (total electron content) of i 0^{19} electrons/m^2, $\Delta\theta$ will be 0.3 mr. Equation (2.33) shows the range error and, therefore the refraction" or elevation angle, to vary inversely with frequency squared.

2. 1.4 QL Approximation

Propagation can occur at any angle θ_B with respect to the magnetic field, and analysis for the general case is more complex than for strictly parallel or perpendicular propagation. The situation is simplified, however, when the QL (quasi-longitudinal) approximation is applicable. To state this approximation, we use the common practice of defining ω_p^2/ω^2 as X and ω_B/ω as Y. Using these quantities, Eqs. (2.1) and '(2,2) take the forms

$$n_l^2 = K_l = 1- x/(1 + Y) \tag{2.18}$$

and

$$n_r^2 = K_r = 1 - X/(1 - Y) \tag{2.19}$$

Also defining Y cos θ_B as Y_L and Y sinθ_B as Y_T, the condition for the QL approximation to apply is

$$4 (1 - X)^2 Y^2 >> Y_T^2 \tag{2.20}$$

When this approximation applies the characteristic waves for propagation at an angle θ_B with respect to the magnetic field are circularly polarized, as they are for $\theta_B = 0$ deg, and their indices of refraction have the forms

$$n_l^2 = K_l = 1 - X/(1 + Y_L) \tag{2.21}$$

and

$$n_r^2 = K_r = 1 - X/(1 - Y_L) \tag{2.22}$$

2.1.5 Application to Space Communications

The value of X in Eq. (2.20) is a major factor in determining if the QL approximation applies, and X is defined as ω_p^2/ω^2. For space communications ω tends to be high, X tends to be small, and the QL approximation tends to apply, even for large values of θ_B. Thus the characteristic waves on earth-space paths are normally left and right circularly polarized waves. Also examination of Eqs. (2. 1) and (2.2) or (2.21) and (2.22) shows that n_l and n_r have values only slightly less than unity for large values of ω and that these values approach closer to unity and to each other as ω increases, Thus for ω sufficiently large, n_l and n_r are essentially unity, reflection does not occur, and the effect of the ionosphere can be neglected. Such is the case for frequencies above 10 GHz. Moving downward in frequency below 10 GHz, however, one reaches frequencies for which ionospheric effects are important, even though n_l and n_r may still be not far from unity,

In this and the following Sees. 2.2 through 2.4 consideration is given to uniform or homogeneous media, but the ionosphere is characterized by various disturbances and irregularities which affect propagation and which are also most important for lower frequencies. These irregularities and their effects are treated in Sees, 2.5 through 2.7.

2.2 FARADAY ROTATION

Anal ysis of the propagation of a linearly polarized high-frequency wave in the ionosphere shows that it experiences rotation of the plane of polarization such that a wave that is launched with vertical polarization, for example, does not remain vertical. Depending on the frequency, length of path in the ionosphere, and orientation with respect to the Earth's magnetic field, the amount of rotation may vary from a negligible amount to amounts in excess of 360 deg to many complete rotations. The basis for such rotation, known as Faraday rotation, is that a linearly polarized wave consists of left and right circularly polarized components which have different indices of refraction. That such is the case can be visualized with the aid of Fig. 2.4.

Consider that E_l and E_r are the electric field intensity vectors" of left and right circularly polarized waves. . Small auxiliary arrows are used to indicate the direction Of rotation for E_l and E_r for a right-handed coordinate system with z, the direction of propagation, extending out of the plane of the page. E_l and E_r are the circularly polarized components of a linearly polarized wave having its electric field intensity in the x direction. Figure 2.4a shows an instant when E_l and E_r both lie on the x axis, an Fig.2.4b shows conditions an instant later. It can be recognized that as the two vectors rotate their projections on the y axis cancel and the sum of their projections on the x axis provide cosinusoidal variation of the amplitude of E, with E always lying along the x axis. Note" that as E varies cosinusoidally, E_l and E_r maintain constant lengths.

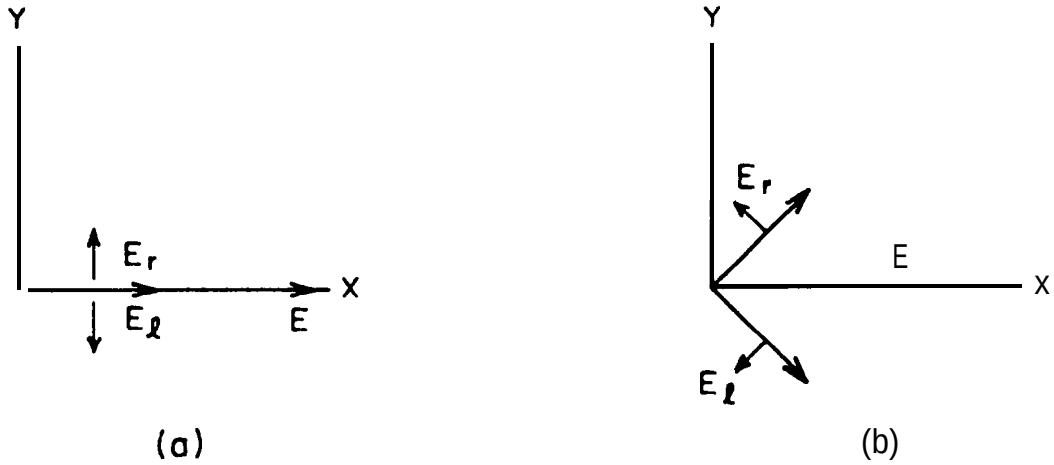

Figure 2.4. Illustration suggesting how circularly polarized waves combine to form a linearly polarized wave.

As the vectors E_l and E_r propagate in the z direction, they continue to rotate with angular velocity ω in their respective directions but the phases of the rotations lag in accordance with the factors $e^{-j\beta_l z}$ and $e^{-j\beta_r z}$. The indices n_l and n_r have different values and therefore β_l and β_r have different values, in accordance with Eq. (2. 13). Thus after propagating a distance z, the rotations are no longer symmetrical about the x axis, and the field intensity E

no longer lies along the x axis but at an angle ϕ from the original x axis where, for the case of a uniform ionosphere

$$\phi = (\beta_l z - \beta_r z)/2 \tag{2.23}$$

[More generally $\phi = \int (\beta_l - \beta_r)/2 \, dz$, with β_l and β_r functions of position along the path.] The parameter β_l is larger than β_r but its lag in phase of rotation is in the right circular direction. Thus Fig. 2.5 shows a possible condition after propagation through some distance z, namely rotation of E through an angle ϕ in the right circular direction.

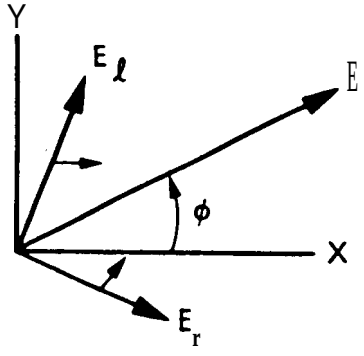

Figure 2.5. Faraday rotation through an angle ϕ from the conditions of Fig. 2.4.

Consider now propagation at an angle θ_B with respect to the magnetic field when the QL approximation applies. For sufficiently high frequencies the calculation of rotation can be simplified by noting that

$$\frac{\beta_0 (n_l - n_r)}{2} = \frac{\beta_0}{2} \left[\left\{ 1 - \frac{X}{1 + Y_L} \right\}^{1/2} - \left\{ 1 - \frac{X}{1 - Y_L} \right\}^{1/2} \right]$$

$$\simeq \frac{\beta_0}{2} \left[1 - \frac{X}{2(1 + Y_L)} - 1 + \frac{X}{2(1 - Y_L)} \right] = \frac{\beta_0}{2} X Y_L \tag{2.24}$$

The electron density and magnetic field along the path will in general not be uniform but total rotation can be determined by first defining the differential rotation $d\phi$ in an increment of path length $d\ell$ and then integrating along the length of path. Thus

$$d\phi = (\beta_0/2)\, XY_L\, d\ell \qquad \text{rad} \qquad (2.25)$$

and, using the definitions of X and Y_L, the total rotation ϕ in radians along a path is given by

$$\phi = \frac{e^3}{2c\epsilon_0 m^2 \omega^2} \int N B \cos\theta_B \, d\ell \qquad \text{rad} \qquad (2.26)$$

where e = 1.6022 x 10^{-*9} C, m = 9.1096 x 10^{-31} kg, c ≃ 3 x 10^8 m/s, ϵ_0 = 8.854 x 10^{-12} F/m, and $\omega = 2\pi f$. Also

$$\phi = (2.36 \times 10^4/f^2) \int N\ B \cos\theta_B\, d\ell \text{ rad} \qquad (2.27)$$

with f in Hz, N standing for electrons/m^3, and B. the Earth's field in Wb/m^2. It should be kept in mind that Eqs. (2.24) - (2.27) are approximations that are valid only at sufficiently high frequencies, perhaps above about 100 MHz.

The total rotation can be seen to vary inversely with f^2 and to be proportional to the integral of electron density, weighted by the value of B cos θ_B along the path. If it is desired. to carry out integration in the vertical direction, letting $d\ell$ = dh, but the path is a slant path, a factor sec χ can be introduced inside the integral, where χ is the zenith angle or angle of the path measured from the vertical. B varies inversely with the cube of the radius from the Earth's center and has very low values above about 2000 km, and Faraday rotation is insensitive to ionization above that level. Therefore Faraday rotation measurements of signals from geostationary satellites provide a measure of ionospheric total electron content but not of total electron content along the entire path to a satellite. The region above the ionosphere, above about 2000 km, may have an electron content that is about 10 percent of the ionospheric content in the daytime and 50 percent at night [Davies, Hartmann, and Leitinger, i 977).

For some situations, it is sufficiently accurate to replace B cos θ_B in Eq. (2.27) by an average value, namely B_L, and to take it outside the integral. The expression for the Faraday rotation angle then becomes

$$\phi = (2.36 \times 10^4/f^2) B_L \int N \, dl = (2.36 \times 10^4/f^2) B_L \ TEC \quad (2.28)$$

with $B_L = (\int N B \cos \theta_B \, dl) \setminus \int N \, dl$. The quantity TEC stands for total ionospheric electron content along the path in this case, - Equation (2. 28) can be inverted to find TEC by use of

$$TEC = \phi f^2/(2.36 \times 1 0^4 B_L) \quad (2.29)$$

On a fixed path, when the above procedure is applicable, the amount of Faraday rotation depends on TEC, which exhibits a pronounced diurnal variation as well as a variation with the season, solar flare activity, and period of the solar cycle. When the form of the variation of electron density with altitude changes the value of B_L may change also.

A practical consequence of Faraday rotation is that, in the frequency range where Faraday rotation is significant, one cannot transmit using one linear polarization and receive using an antema with the same linear polarization without a high probability of a significant polarization loss. Among the techniques for avoiding or dealing with the problem are using a sufficiently high frequency that Faraday rotation is negligible, using a receiving antenna that can accept both orthogonal linear polarizations so that no polarization loss occurs, and using circular rather than linear polarization. As a right or left circularly polarized wave is a characteristic wave, it does not change polarization as it propagates and thus presents no problem, as long as both antennas of the link are designed for the same circular polarization. Another possibility, if Faraday rotation is not too great or highly variable, is to vary the orientation of a linear transmitting or receiving antenna to compensate for the Faraday rotation expected along the path, as a function of time of day, season, and period of the sunspot cycle,

As Faraday rotation and group delay and other topics of the following Sec. 2.3 are all functions of TEC (total electron content) along a path, numerical illustrations of Faraday rotation are deferred until Sec. 2.4 which deals with TEC.

2.3 GROUP DELAY, PHASE ADVANCE, DOPPLER FREQUENCY, AND BANDWIDTH COHERENCE

2.3.1 Group Delay

To consider excess ionospheric group delay, or excess range delay, at high frequencies, note that the integral $\int n\,dl$, evaluated along a path with n representing index of refraction, gives the true distance along the path if n = 1 but gives a value, sometimes called the phase path length, which is different from the true distance if n does not equal unity. Thus AR, the difference between P and the true length R, is given by

$$AR = \int (n - 1)\, dl \tag{2.30}$$

Neglecting refraction and considering that f > 100 MHz so that $n^2 \simeq 1 - X$,

$$n^2 = 1 - f_p^2/f^2 = 1 - 80.6\ N/f^2 \tag{2.31}$$

where N is electron density (el/m^3) and f is frequency in Hz. Taking X as being small compared to unity as is the case for sufficiently high frequencies (f > 100 MHz),

$$n \simeq 1 - X/2 = 1 - 40.3\ N/f^2 \tag{2,32}$$

For group delay, however, one is concerned with the group velocity rather than phase velocity. As $v_g v_p = C^2$ for ionospheric propagation when $V_p > c$, where V_g is group velocity and V_p is phase velocity, one should use the group refractive index, $n_g = 1 + X/2$. The result is that

$$AR = \frac{40.3}{f^2} \int N\, dl \qquad m \tag{2.33}$$

where AR is a positive range error (excess range delay) and is the difference between the true range and that which would be inferred by assuming a velocity of c. (The true range is less than the inferred range.) The excess range delay AR corresponds to an error in time or an excess time delay of

$$\Delta t = \frac{40.3}{cf^2} \int N \, dl = \frac{1.34 \times 10^{-7}}{f^2} \int N \, dl \quad s \qquad (2.34)$$

where $\int N \, dl$ is the TEC (total electron content) along the path. If the TEC is known or can be estimated closely, At can be determined from Eq. (2.34).

Use of a second lower frequency allows determining At and TEC without any advance information. Let $\Delta t_1 = 40.3 \, TEC/cf_1^2$ where f_1 is the frequency of major interest and let $\Delta t_2 = 40.3 \, TEC/cf_2^2$. Then

$$\delta t = \Delta t_2 - \Delta t_1 = \frac{40.3 \, TEC}{c} \left[\frac{1}{f_2^2} - \frac{1}{f_1^2} \right] \qquad (2.35)$$

It is now possible to solve for Δt_1 which is given by

$$\Delta t_1 = \frac{f_2^2}{f_1^2 - f_2^2} \delta t \qquad (2.36)$$

The quantity δt can be readily measured by suitably modulating both carrier frequencies but At cannot be measured directly for lack of a suitable reference.

Equation (2.35) can be rearranged to give the value of TEC, i.e.

$$TEC = \frac{\delta t \, c}{40.3} \frac{f_1^2 f_2^2}{f_1^2 - f_2^2} \qquad (2.37)$$

A procedure has been described for determining Δt at the expense of utilizing a second frequency. Such a correction is important in the case of satellite positioning systems such as the GPS (global positioning system). Using GPS it may be possible to determine position to an accuracy of a few meters, whereas if no allowance is made a TEC of $10^{18}/m^2$ can cause an error of 134 ns or 40 m at a frequency of 1 GHz (Klobuchar, 1978).

Another case where high accuracy is desired is that of the DSN (Deep Space Network,) of the Jet Propulsion Laboratory, where it may be desired to determine ranges to spacecraft with an accuracy of 3 m or better. Coded signals are transmitted to spacecraft at S or X band and retransmitted back to the station at X band. Also range measurements are used for determining the declination angle of a spacecraft near zero declination by VLBI techniques. This procedure involves determining the difference in distance to the spacecraft from Goldstone, California and Canberra, Australia. Correction for excess time delay is essential for this purpose.

Equation (2.37), when applied to an earth-space path, gives the TEC along the entire path, in contrast to Faraday rotation measurements which give the electron content of the ionosphere only. Numerical values of time delay are given in Sec. 2.4.

2.3.2 Phase Advance

The presence of the ionosphere advances the phase ϕ of a received signal with respect to the value for unionized air. (Do not confuse phase with Faraday rotation." The same symbol # is used here for these two different phenomena.) The phase advance $\Delta\phi$ can be found by multiplying the excess range delay ΔR by the phase constant $\beta = 2\pi/\lambda = 2\pi f/c$, with the result that

$$\Delta\phi = \frac{40.3\ (2\pi f)}{f^2\ c}\ \text{TEC} = \frac{8.44 \times 10^{-7}}{f}\ \text{TEC rad} \qquad (2.38)$$

Dividing by 2π gives the value of $\Delta\phi$ in cycles.

$$\Delta\phi = \frac{1.34 \times 10^{-7}}{f}\ \text{TEC cycles} \qquad (2.39)$$

2.3.3 Doppler Frequency

Frequency and phase are related by

$$f = \frac{1}{2\pi} \frac{d\phi}{dt} \qquad (2,40)$$

with f in Hz and ϕ in radians. The Doppler shift in frequency, f_D, corresponding to the phase change of Eq. (2.39) is given by

$$f_D = \frac{1}{2\pi} \frac{8.44 \times 10^{-7}\, d(TEC)}{f \quad dt} - \frac{1.34 \times 10^{-7}\, d(TEC)}{f \quad dt}$$

In terms of finite quantities

$$f_D = \frac{1.34 \times 10^{-7}\, \Delta(TEC)}{f \quad T_c} \qquad (2.41)$$

where the TEC changes by A (TEC) in the time interval or count time T_c and f_D is the average value during T_c.

2.3.4 Difference Range versus Integrated Doppler

A technique known as differenced range versus integrated Doppler (DRVID) has been used at the Jet Propulsion Laboratory for obtaining information about changes in columnar electron content (TEC) (Callahan, 1975). The basis for the technique is the difference in group and phase velocities, the group velocity being less than c and the phase velocity being greater than c, In terms of index of refraction,

$$n_g = 1 + 40.3\ N/f^2 \text{ and } n = 1 - 40.3\ N/f^2$$

where n_g is the group index and n is the phase index (which is normally what one refers to when speaking of index of refraction), Total columnar electron content TEC and electron density N are related by TEC = $\int N\, dl$, where the integral is taken along the path length,

The Deep Space Network of the Jet Propulsion Laboratory has utilized a system for measuring range delay by the use of two-way transmissions of coded pulse trains. For the time interval between to and t, this system provides a value AR which is a combination of a true change in range, $R(t) - R(t_o)$, and the excess range delay 40.3 A (TEC)/f^2. That is

$$ARg(t, to) = R(t) - R(t_o) + \frac{40.3\ \Delta(TEC)}{f^2} \qquad (2.42)$$

A similar expression applies for $\Delta R_\phi(t,t_o)$, which is obtained from a phase or Doppler frequency measurement .

$$\Delta R_\phi(t, t_o) = R(t) - R(t_o) - \frac{40.3\ \Delta(TEC)}{f} \qquad (2.43)$$

The difference $\Delta R_g - \Delta R_\phi$ is designated as DRVID and is given by

$$DRVID\ (t, t_o) = AR_g - \Delta R_\phi = \frac{80.6\ \Delta(TEC)}{f^2} \qquad (2.44)$$

The change in TEC, Δ(TEC) can be determined from Eq. (2.44), and if a series of consecutive measurements of this kind are made a record of the variation of TEC can be-constructed, Note that the absolute value of TEC can not be determined by this method but that the effects of motion of the spacecraft and of the troposphere are canceled out as n_g and n are the same in the troposphere.

The quantity ΔR_ϕ can be obtained from the expression, in terms of finite increments of phase and time, for Doppler frequency f_D, namely

$$f_D = \frac{1}{2\pi} \frac{\Delta\phi}{T_c} \qquad (2.45)$$

and from the expression relating $\Delta\phi$ and ΔR_ϕ, which is

$$\Delta\phi = \frac{2\pi}{\lambda_o} AR_\phi \tag{2.46}$$

By substituting Eq. [2.46) into Eq. (2.45), $\Delta\phi$ can be eliminated, with the result that

$$f_D = \frac{1}{\lambda_0} \frac{AR_\phi}{T_c} \quad \text{or} \quad AR_\phi = f_D \lambda_o T_c \tag{2.47}$$

2.3.5 Bandwidth Coherence

The rate of change of time delay with frequency, or the time-delay dispersion, is found by taking the derivative of Eq. (2.34) yielding

$$\frac{dt}{df} = \frac{-80.6}{cf^3} \int N\,dl = \frac{-2.68 \times 10^{-7}}{f^3} \text{ TEC} \tag{2.48}$$

The rate of change of phase angle with frequency, or the phase dispersion, is found by taking the derivative of Eq. (2.38) giving

$$\frac{d\phi}{df} = \frac{-8.44 \times 10^{-7}}{f^2} \text{ TEC} \tag{2.49}$$

The effect of dispersion is to introduce distortion into broadband signals.

2.4 ELECTRON CONTENTS OF IONOSPHERE AND PLASMASPHERE AND THEIR EFFECTS

Faraday rotation measurements on satellite-to-Earth paths provide values of the electron content of the ionosphere, and group delay measurements give the total electron content (TEC) along the entire path. By taking the difference of the total and ionospheric

values, the electron content of the plasmasphere or protonosphere is obtained. Most electron content data refer to ionospheric values, but data for the plasmasphere as well have been reported by Davies, Hartman, and Leitinger (1977), Klobuchar and Working Group (1978), and Davies (1980).

The ionospheric TEC shows pronounced diurnal variations consistent with the production of ionization by solar radiation in the daytime and the decay of ionization at night. 'Extreme values of the ionospheric TEC are given by Klobuchar (1978} as $10^{16}/m^2$ and $10^{19}/m^2$; 1018,~m2 is generally regarded as the maximum zenith value, Zenith values of ionospheric TEC refer to the electron content of a vertical column having a cross section of one square meter and extending to the height of the plasm asphere. Representative curves showing the diurnal variation of TEC for an invariant latitude of 54 deg are given in Fig. 2.6. Invariant latitude equals $\cos^{-1}(1/L)^{*'^2}$ and refers to the magnetic field line that is at a distance L, measured in earth radii, from the center of the Earth at the magnetic equator. The data were obtained at Sagamore Hill, MA using 136 MHz signals from ATS-3.

One effect of TEC is to produce excess group time delay. Plots showing ionospheric time delay as a function of TEC and frequency are shown in Fig. 2.7. A worldwide model giving ionospheric time delay at a frequency of 1.6 GHz is shown in Fig. 2.8. Typical values of Faraday rotation as a function of ionospheric TEC and frequency for a nort hem mid-latitude earth station viewing a geostationary satellite near the station meridian are shown in Fig. 2.9. Using Fig. 2.6 together with Figs. 2.7 and 2.9 provides information about the diurnal variation of TEC and how this variation affects time delay and Faraday rotation. Ionospheric disturbances and irregularities and the solar cycle also cause variations in these parameters that may be important in some cases.

Table 2.2 gives a summary of ionospheric effects at frequencies from 100 MHz to 10 GHz. Included are the effects of Faraday rotation, time delay, refraction, and dispersion that have already been mentioned and values for absorption and variation in direction of arrival.

Table 2.2 Estimated maximum ionospheric effects in the United States for one-way paths at an elevation angle of about 30 deg [derived from CCIR Reports 565-3 (CCIR, 1986a), 263-4, 263-5, and 263-6 (CCIR, 1986b).]

Effect	100 MHz	300 MHz	1 GHz	3 GHz	10 GHz
Faraday rotation	30 rot.	3.3 rot.	108°	12°	1.1°
Excess time delay	25 μs	2.8 μs	0.25 μs	0.028 μs	0.0025 μs
Refraction	≤ 1°	<7 min	≤0.6 min	<4.2 s	≤0.36 s
Variation in direction of arrival	20 min	2.2 min	12 s	1.32 s	0.12 s
Absorption (auroral and polar cap)	5 dB	1.1 dB	0005 dB	6×10^{-3} dB	5×10^{-4} dB
Absorption (mid latitude)	<1 dB	0.1 dB	(0.01 dB	<I X1 O-3 dB	$<10^{-4}$ dB
Dispersion	0.4 ps/Hz	0.015 ps/Hz	0.0004 ps/Hz	1.5×10^{-5} ps/Hz	4×10^{-7} ps/Hz

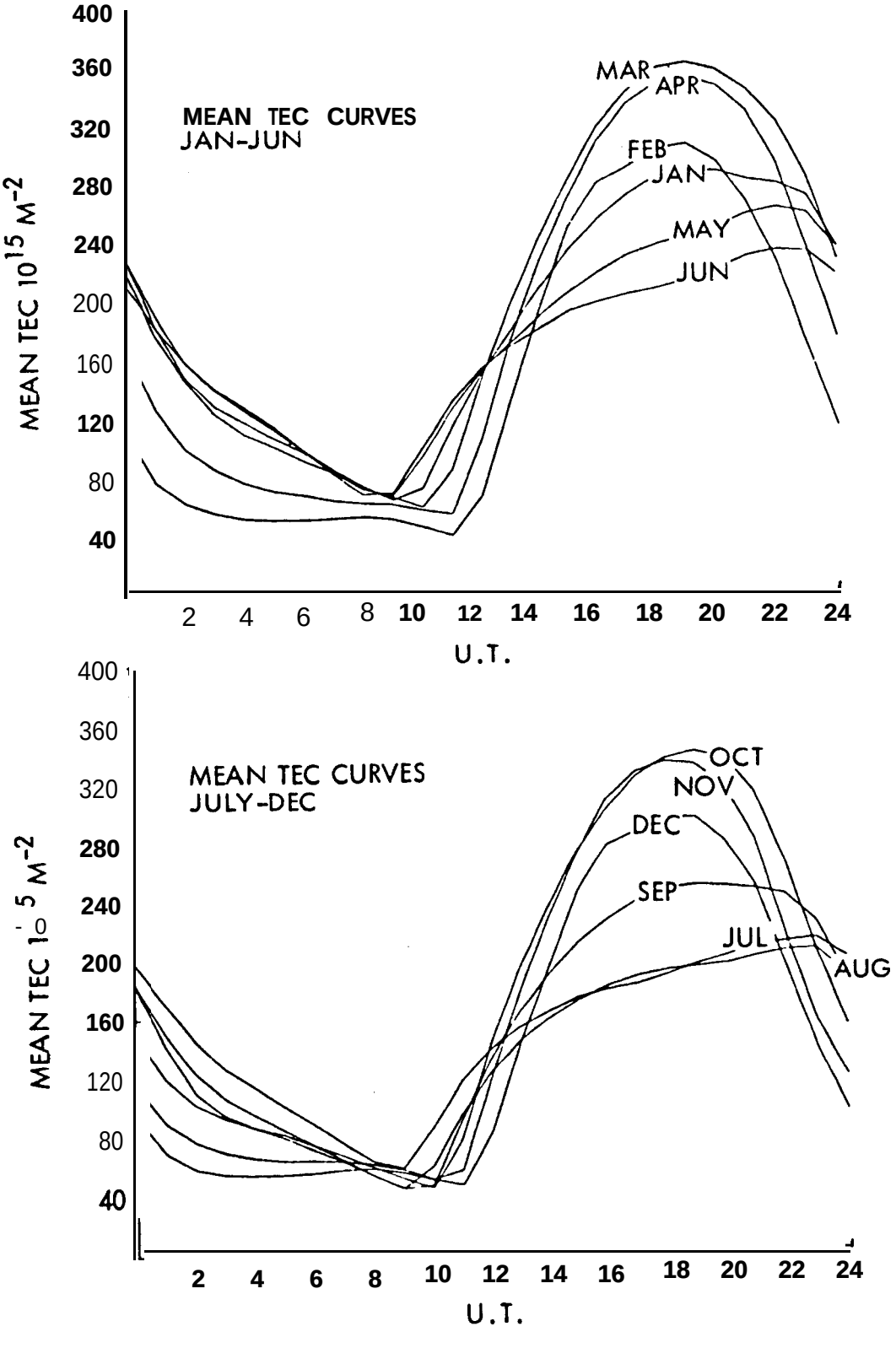

Figure 2.6 Diurnal variations in TEC, mean monthly curves for 1967 to 1973 as obtained at Sagamore Hill, MA . (after Hawkins and Klobuchar, 1974).

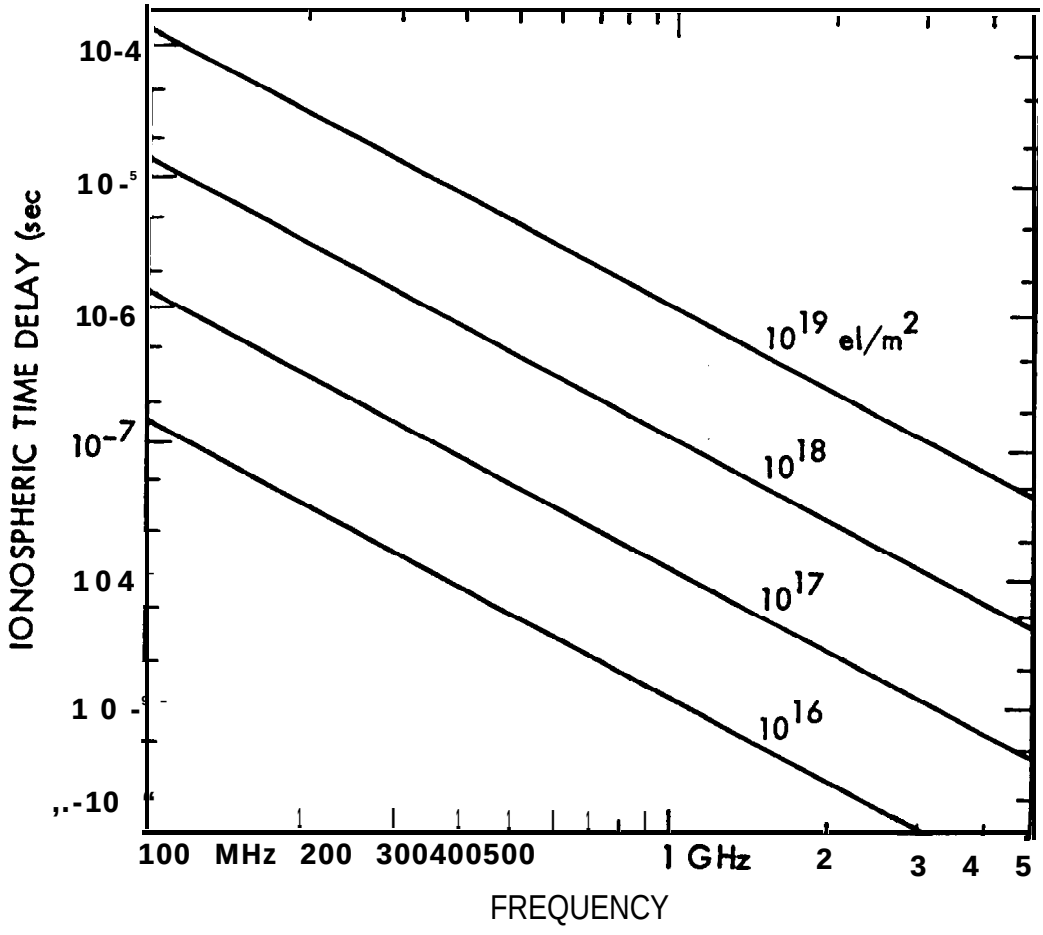

Figure 2.7. Ionospheric time delay as a function of ionospheric TEC and frequency (after Klobuchar, 1978).

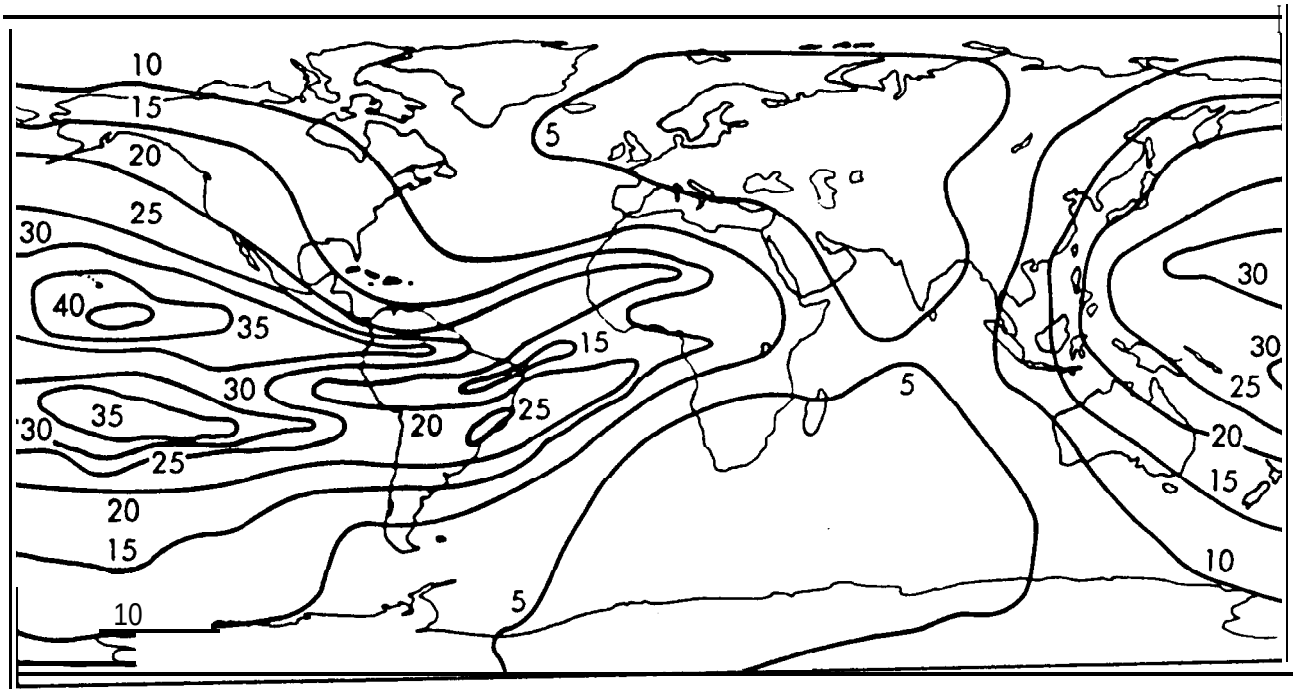

Figure 2.8. Ionospheric time delay in nanoseconds at a frequency of 1.6 GHz, based on the Bent model of ionospheric TEC (after Klobuchar, 1978).

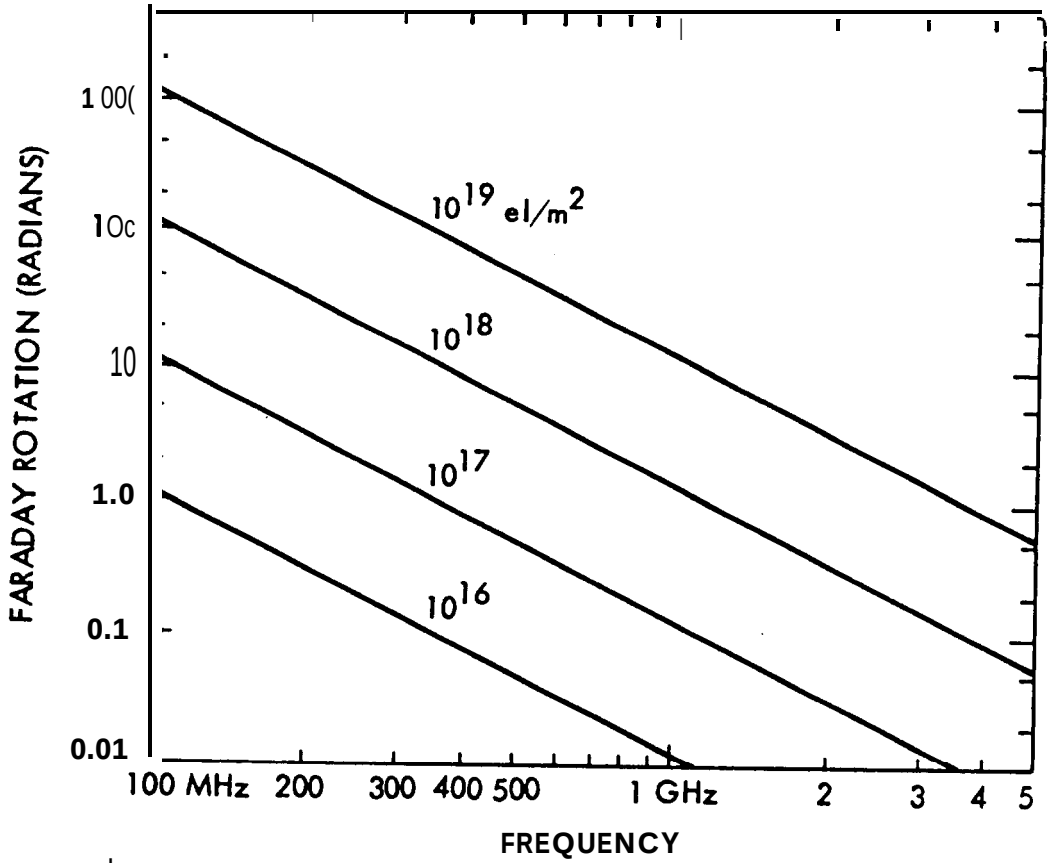

Figure 2.9. Faraday rotation as a function of ionospheric TEC and frequency (after Klobuchar, 1978).

2.5 IONOSPHERIC DISTURBANCES AND IRREGULARITIES

Z. 5.1 Equatorial Ionosphere

Because of atmospheric solar and lunar tidal forces and heating by the Sun, horizontal movements or winds occur in the ionosphere. As a result. electric fields are developed by the dynamo effect, described by" E = vx B, where E is electric field intensity, v is the velocity of the charged particles of the ionosphere, and B is the Earth's magnetic field. (This is a vector relation and E is perpendicular to both v and B.) The electric fields in turn drive a current system in the ionosphere which involves two systems of current loops in the daytime hemisphere, one in the northern hemisphere and one in the southern hemisphere. The currents flow counterclockwise in the northern hemisphere and clockwise in the southern hemisphere so that the currents of both systems flow from west to east near the geomagnetic equator. It develops that the conductivity becomes high overa restricted range of altitude in this equatorial region. In addition the equatorial ionosphere is favorably situated to intercept solar radiation, which is the main agent causing ionization in the ionosphere. As a result of the factors mentioned, a strong, concentrated current, known as the equatorial electrojet, flows at heights from 90 to 130 km in the E region of the equatorial ionosphere. Electron density irregularities and variations associated with the electrojet cause scattering of electromagnetic waves which are incident upon and propagate through this region. Strong radar backscatter echoes are received from the equatorial electrojet. The Jicamarca Radar Observatory near Lima, Peru, operating at a frequency near 50 MHz, has provided a large amount of information concerning the equatorial ionosphere. It can record both discrete echoes from E and D irregularities and weak incoherent-scatter echoes from the entire ionosphere (Evans, 1969, Farley, 1963, Balsley, 1969).

The occurrence of plasma bubbles (McClure et al., 1977) has been an object of investigation since Woodman and La Hoz (i 976) reported the appearance of rising plume-like structures, using the Jicamaraca radar. The bubbles typically have a width of 100 km and electron densities 1 to 2 orders of magnitude less than the surroundings (Heron, 1980). Such bubbles are considered further in Sec. 2.6.

2.5.2 Auroral Ionosphere

Energetic particle precipitant ion into the auroral ionosphere causes the visible aurora, excess ionization which attenuates and scatters radio waves, and concentrated electrical currents known as auroral electrojets. The currents in turn cause characteristic variations in the geomagnetic field. These phenomena occur in the form of an oval (fig. 2. 10) which surrounds but is eccentric with respect to the Earth's magnetic dip pole, with the oval center displaced by about 3 deg toward the dark hemisphere (Akasofu, 1968). The oval is fixed approximately with respect to the Sun, and the Earth rotates beneath the oval. The term auroral zone is applied to the area that is swept out by the midnight portion of the auroral oval, where auroral activity occurs essentially every night to some degree. The concept of the auroral oval has been reviewed recently by Feldstein (1986).

The excess ionizat ion occurs prominent y in th? E region and can be regarded as a variety of sporadic E. Intense radar backscatter or radar auroral echoes can be received at HF, VHF, and UHF frequencies. The irregularities in ionization are field aligned, having a considerable extent along the Earth's magnetic field lines and a small extent perpendicular to the lines. The line of sight to the echoing region must be close to perpendicular to the magnetic field to receive VHF-UHF echoes which must therefore be at ranges of 500-900 km in Alaska. An auroral radar facility at Anchorage, Alaska has transmitted data to the NOAA-USAF Space Environment Services Center in Boulder, Colorado. HF waves experience sufficient refraction in the auroral ionosphere to achieve perpendicularity without being launched originally in the perpendicular direction. An ionospheric trough, namely a region of reduced ionization, separates the auroral and mid-latitude ionospheres, This trough appears to be linked by magnetic field lines to the plasmapause of the magnetosphere (Sec. 1.3).

The riometer (relative ionospheric opacity meter) has been a valuable tool for studying the auroral and polar ionospheres. It operates typically at a frequency of 30 MHz and, by recording the amplitude of cosmic noise, monitors auroral and polar-cap activity and the associated attenuation experienced by radio waves propagating through the auroral ionosphere. An incoherent scatter radar facility at Chatanika, Alaska near Fairbanks, has been in

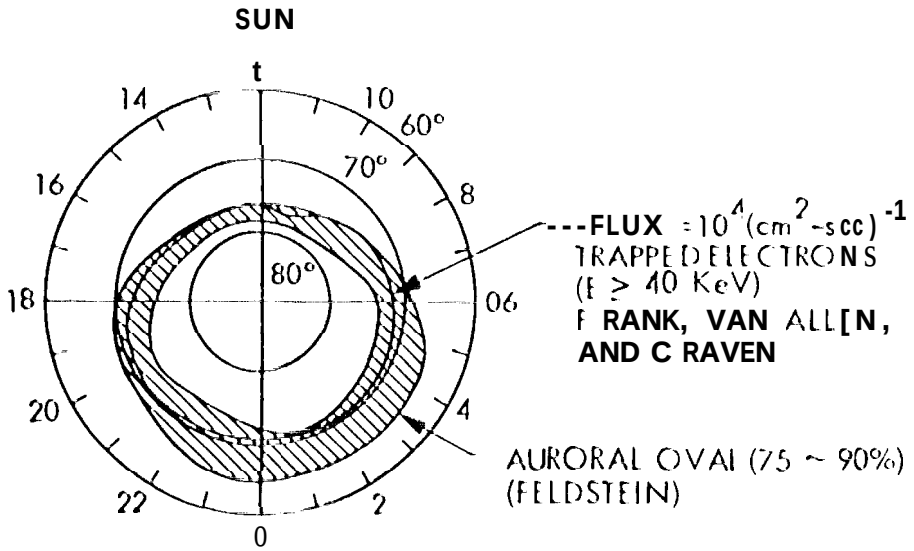

Figure 2.10. The auroral oval (Akasofu, 1968).

operation since about 1972 and has provided extremely valuable information about the auroral ionosphere (Leadabrand et al., 1972; Baron, 1974; Hunsucker, 1974). Auroral absorption is considered further in Sec. 2.7.

2.5.3 SID'S and ionospheric Storms

The equatorial and auroral ionospheres are characterized by irregularities and disturbed conditions on a more or less continuous basis, but, varying as to degree and subject to diurnal variation. The mid-latitude ionosphere exhibits less activity and disturbance generally but is subject to the effects of solar flares and sporadic E. Auroral activity is also enhanced by flare activity.

The effects of solar flares can be divided into the categories of simultaneous and delayed. The simultaneous effects result from the radiation of X-rays from the flares. X-rays propagate with the velocity c, the velocity of light. The simultaneous effects are known as sudden ionospheric disturbances (SID's), a term which covers a variety of phenomena including SWF (shortwave fadeout), SCNA (sudden cosmic noise absorption), SPA (sudden phase anomaly) and SFD (sudden frequency deviation). These effects tend to be important at HF frequencies. Phase ϕ and frequency f are related by

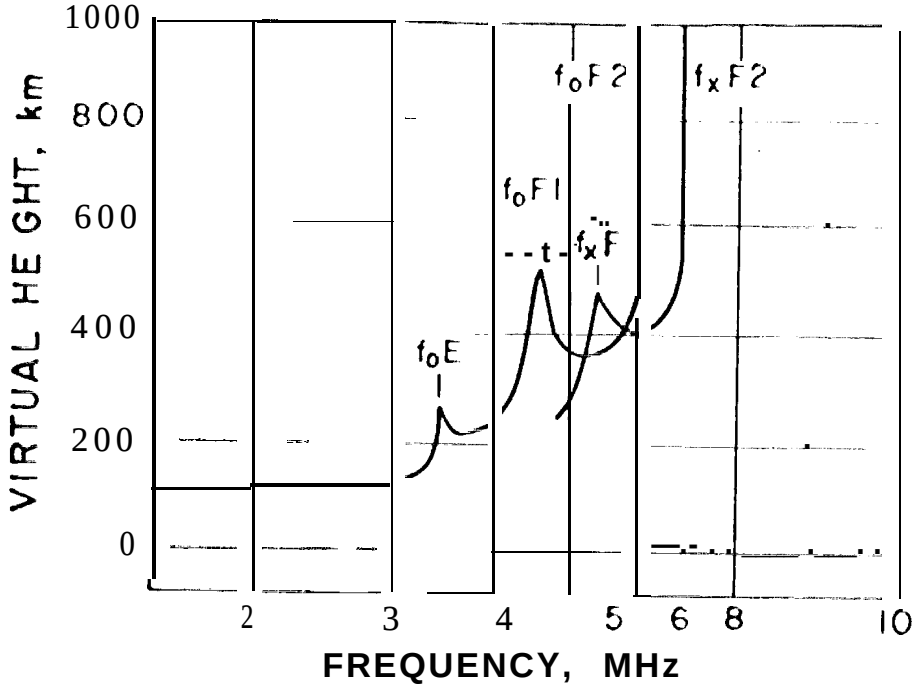

Figure 2.11. Ionospheric traces under quiet ionospheric conditions, Washington, DC. June 3, 1962 (after Davies, 1969).

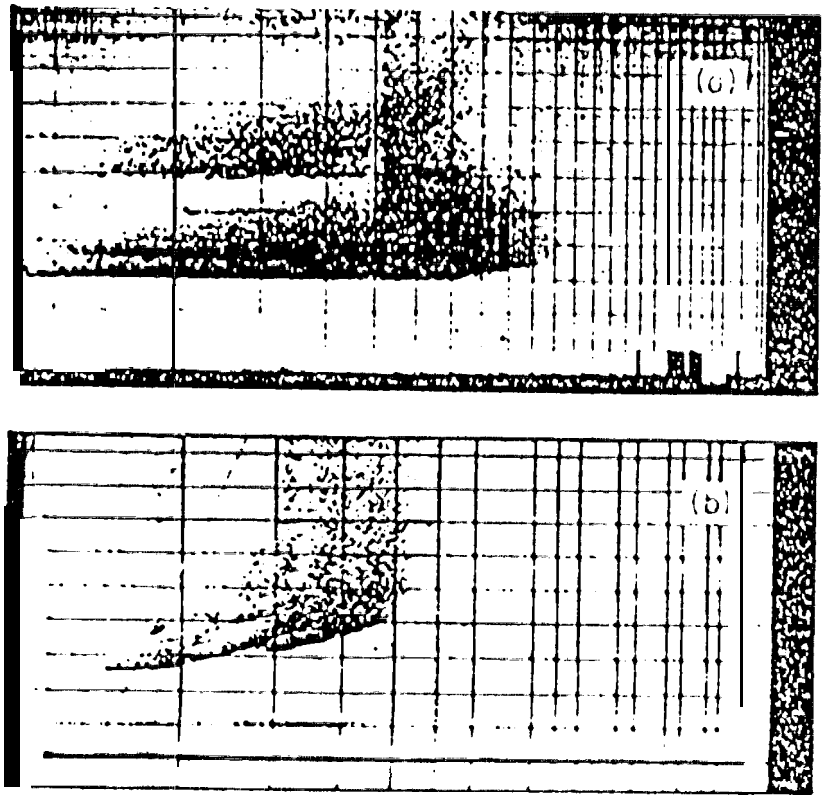

Figure 2.12. Ionograms showing spread-F. a. Range spreading. b. Frequency spreading. Virtual height versus frequency. (Davies, 1965).

2.6 IONOSPHERIC SCINTILLATION

2.6.1 Introduction

Irregular variations or scintillations of the amplitude of radiowaves from radio stars were first recorded by Hay, Parsons, and Phillips (1946) who reported variations in the amplitude of signals from **Cygnus** and Cassiopeia at 36 MHz. At first, it was thought that the emissions from the stars might be varying with time, but records obtained simultaneously from stations separated by 200 km showed no similarity whereas when the receiver separation was only about 1 km the records were closely similar (Smith, 1950; Little and Lovell, 1950). These results showed that the scintillations were not caused by the stars but were of localized origin, and it was concluded that their source was in the ionosphere. The scintillations were attributed by Hewish (1952) to a diffraction pattern formed at the ground by a steadily drifting pattern of irregularities in the ionosphere at a height of about 400 km. According to Aarons, Whitney, and Allen (1971), the irregularities are mostly in the F layer at heights predominantly from 225 to 400 km.

With the advent of satellites, scintillations of signals from such spacecraft were also observed (Yeh and Swenson, 1964). The signals from radio stars are incoherent and broadband and allow the recording of amplitude and angle-of-arrival stint i 1 lat ions but not phase scintillations. Coherent, monochromatic signals from spacecraft have the advantage. of. allowing the recording of phase scintillations and spectral broadening as wellas amplitude scintillations (Crane, 1977; Woo, 197"7; Smith and Edelson, 1980). The early observations of scintillations were at comparatively low frequencies and, on the basis of the assumed form of decrease of scintillation intensity with frequency, it was expected that frequencies as high as those of the 4 and 6 GHz bands planned for the INTELSAT system would be free from scintillation effects. It developed, however, that scintillation occurs at 4 and 6 GHz at equatorial latitudes (Craft and Westerlund, 1972; Taur-, 1973).

Stint illation may involve weak scattering or strong scattering. The strongest scattering is observed in the equatorial and auroral regions, especially the equatorial areas. The resulting scintillation

is correspondingly intense and extends to higher frequencies than elsewhere. Scintillation tends to be weak at temperate latitudes. Maximum scintillation occurs at night in all three regions. The pattern of occurrence is suggested in Fig. 2.13. It is generally agreed that the weak mid-latitude scintillation is due to diffractive scattering, and it has sometimes been assumed that such is the case for all scintillation. Certain analyses of strong scattering, including that responsible for scintillation at microwave (SHF) frequencies, however, have led to conclusions that such scintilla ion must be caused by a higher portion of the atmosphere, in particular the plasmasphere (Booker, 1975) or by a different mechanism, namely refractive scattering rather than diffractive scattering (Crain, Booker, and Ferguson, 1979). The refractive scattering is said to be caused by ionization structure in the form of "holes" or "bubbles" that are perpendicular to the line of sight. Refractive scattering is considered to involve irregularities of scale larger than the Fresnel scale, and diffractive scattering is assumed to involve irregularities having sizes near the Fresnel scale.

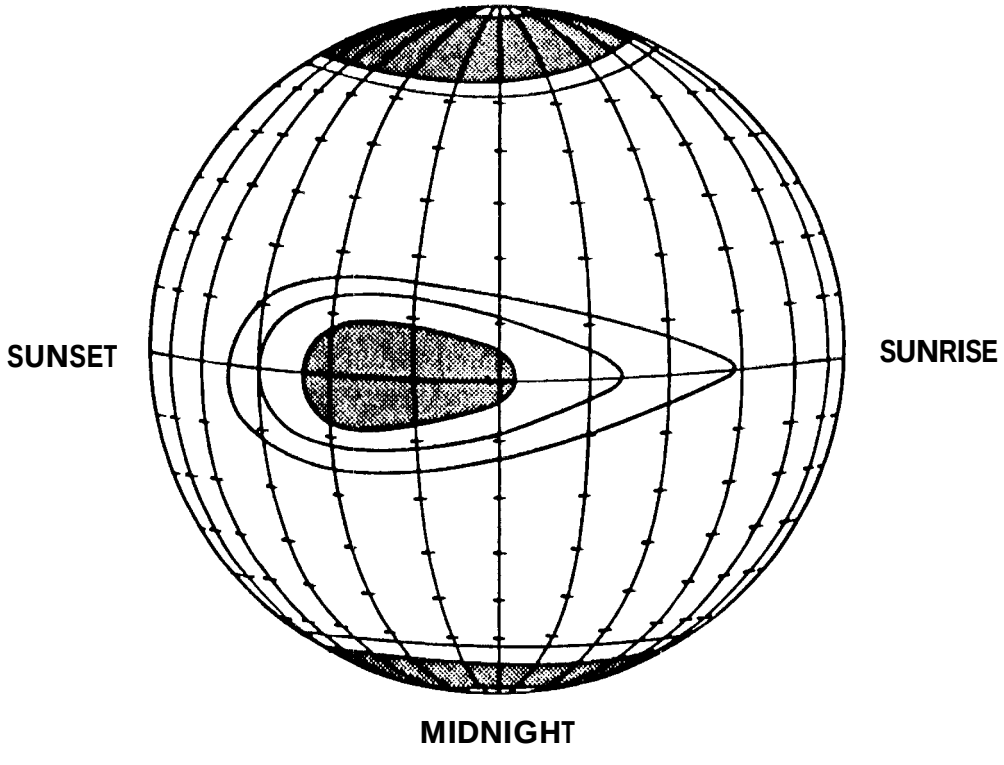

Figure 2.13. Pattern of ionospheric scintillation (CCIR, i 986 b).

Several measures or indices of scintillation have been used. Attention was given to the subject of indices by Briggs and Parkin (1963) who introduced indices designated by S, S_1, S_2, and S_4, The index S_4, representing the standard deviation of received power divided by the mean value is said to be the most useful of the several indices (Klobuchar and Working Group (1978). It is given by

$$S4 = \frac{1}{\overline{E^2}} \left[\frac{}{(E^2 - \overline{E^2})^2} \right]^{1/2} \qquad (2.51)$$

where E is field intensity. A similar index, m, is defined as the ratio of rms fluctuation to mean value of power.

The index S1 has been proposed as a convenient approximate measure of scintillation (Whitney, Aarons, and Malik, 1969). It is defined by

$$SI = \frac{P_{max} - P_{min}}{P_{max} + P_{min}}$$

where the P's represent power. In order to avoid overemphasizing extreme conditions, it is recommended that the third peak down from the maximum and the third minimum up from the absolute minimum be used to define P_{max} and P_{min}.

The parameter τ_c, the fade coherence time, is pertinent to digital communications. If τ_c is long compared to the time interval corresponding to one bit, the average bit error can be computed in terms of S_4. It has been stated that knowledge of S_4, τ_c, and a rough measure of coherence bandwidth are what is needed for considering the effect of scintillation on transionospheric communication systems (K. obuchar and Working Group, 1978).

2.6,2 Theoretical Background

Discussions of ionospheric scintillation may refer to Fresnel scale sizes and distances. To introduce these concepts, consider a path of length d between transmitting and receiving locations, At distances d_T from the transmitter and d_R from the receiver, the first Fresnel zone radius F_1 is given by (Appendix 2.1)

$$F_1 = \left(\frac{\lambda d_T d_R}{d} \right)^{1/2} \qquad (2.52)$$

All the elements of radiation passing through the first Fresnel zone have components of electric field intensity that add constructively. If the distance to the transmitter d_T becomes very large compared to d_R, d_T approaches d and the first Fresnel zone radius is given by

$$F_1 = (\lambda d_R)^{1/2} \qquad (2.52a)$$

The first Fresnel zone is circular in cross section and has an area of πF_1^2, Converting to different symbols, corresponding to irregularities that occur with a radius or scale size L about equal to F_1 at a height h = z above a point of observation Eq. (2.52a) becomes

$$L = (\lambda z)^{1/2} \qquad (2.52b)$$

Upon rearrangement, one obtains

$$z = L^2/\lambda \qquad (2.53)$$

In Eqs. (2.52b) and (2.53), L takes the place of F_1 and z takes the place of d_R. In some cases, one may wish to know the Fresnel distance z corresponding to a certain value of L. In other applications, one may wish to know the Fresnel scale size L corresponding to a certain distance z. If d_T is not sufficiently large to justify using Eq. (2.52 b), one can revert to Eq. (2.52).

Some analyses of ionospheric scintillation are based On consideration of scattering in an ionospheric layer or screen containing identical roughly isotropic or ellipsoidal irregularities of scale size L, as in Fig. 2.14, Let the irregularities of the layer be characterized by AN, the deviation in electron density from that of surroundings. The corresponding deviation An in index of refraction n can be determined by use of Eq. [2.33) to be given by

$$An = - 40.3\ \Delta N/f^2 \tag{2.54}$$

Therefore

$$\overline{(\Delta n)^2} = 1.624 \times 10^3\ \overline{(\Delta N)^2}/f^4 \tag{2.55}$$

where the overbars indicate mean values. The phase change $\Delta\phi$ in traversing a single irregularity of size L is

$$\Delta\phi = (2\pi/\lambda)(L\ An) \tag{2.56}$$

where $2\pi/\lambda$ is the phase constant. Equation [2. 55) can be written in an alternative form as

$$\frac{\overline{(\Delta n)^2}}{n} = \frac{1}{4\pi^2}\ r_e^2\ \lambda^4\ \overline{(\Delta N)^2} \tag{2.57}$$

where r is the classical electron radius (2.82×10^{-15} m). Using this for% and considering a layer of thickness D rather than a layer of negligible thickness, the total mean square phase fluctuation $\overline{(\Delta\phi)^2}$ in a layer of thickness D at a zenith angle χ is given by Booker (1975) as

$$\overline{(\Delta\phi)^2} = 4\ r_e^2\ \lambda^2\ \overline{(\Delta N)^2}\ L\ D \sec\chi \tag{2.58}$$

Note that n of Eq. (2.57) is essentially unity and that Δn can be either a positive or negative quantity. The classical electron radius, r_e, is given in terms of other quantities by $r_e = \mu_o e^2/4\pi m$, (CRC, 1972) where $\mu_o = 4\pi \times 10^{-7}$ H/m is the magnetic

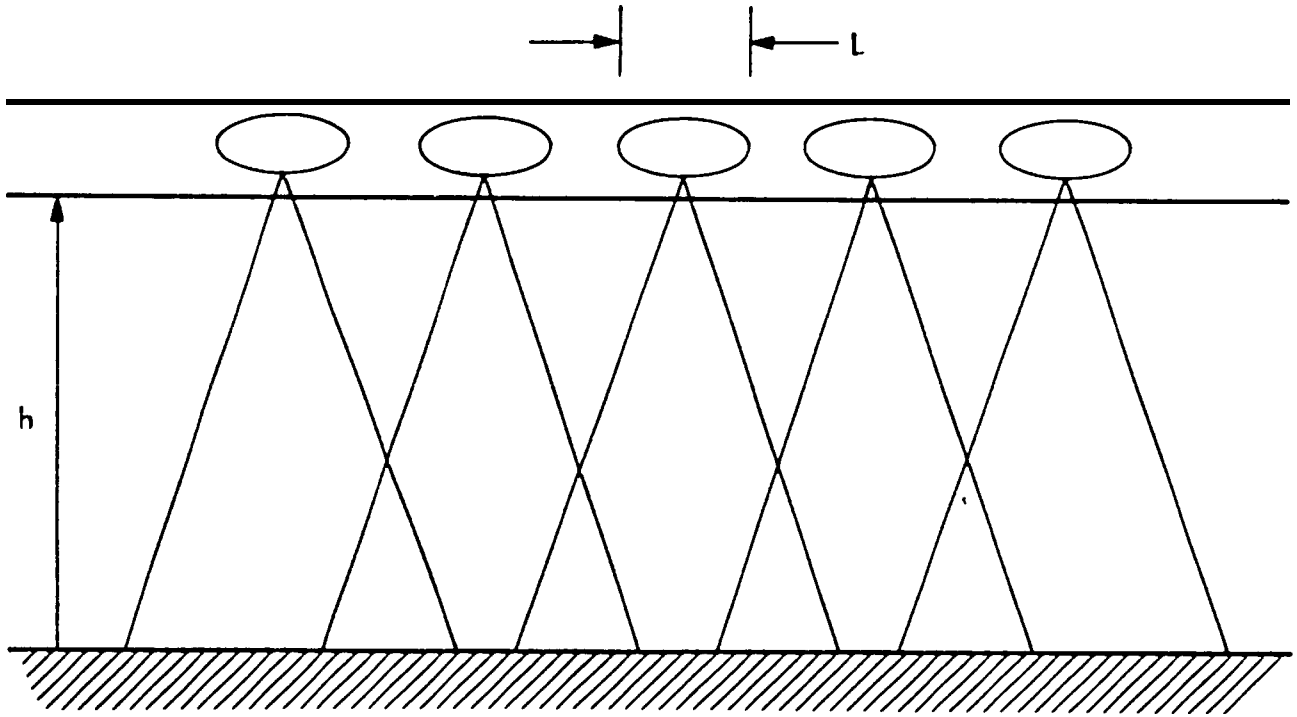

Figure 2.14. Layer of irregularities of scale size L.

permittivity of empty space and e and m are the charge and mass of the electron, respectively. It is not essential that the quant it y classical electron radius be introduced into Eqs. (2.57) and (2.58). Instead one can employ Eq. (2.54) and f = c/λ giving directly the result the that $|\Delta n|^2 = (4\ 484\ X\ 10^{-16})^2\ \lambda^4\ |\Delta N|^2$. [A check of the numerical coefficient of $\Delta N|^2$ shows that it equals $r_e^2/4\pi$.]

Only phase variations occur immediately below the layer of' Fig. 2.14, but amplitude variat ions develop farther below the layer The distance h that is required for amplitude fluctuations to deve op is in the order of the Fresnel distance z = L^2/λ of Eq. (2.53) , In particular, if h ? $\pi L^2/\lambda$ amplitude fluctuations are sa d to develop '(Booker, 1975). The phasor diagram of Fig. 2.15 can help to visualize the association of phase and amplitude fluctuations The parameter A represents the undisturbed component of field intensity

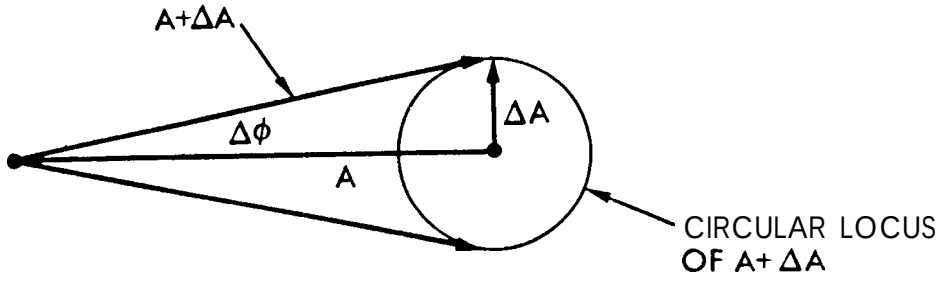

Figure 2.15 Phasor illustration of amplitude and phase variations.

and $\overline{(\Delta A)^2} = \overline{(\Delta\phi)^2}\ A^2$ so that

$$\overline{(\Delta A/A)^2} = \overline{(\Delta\phi)^2} \qquad (2.59)$$

in the fully developed case. In the diagram AA represents a quantity that adds with random phase to A to produce amplitude variations.

Using results obtained by Bowhill (1961) but expressing relations in his own notation, Booker (1975) obtained the following expressions for phase and amplitude scintillations for weak scattering. The relations are in terms of $Z = \pi L^2/\lambda$.

$$\overline{(\Delta\phi)^2} = 4\, r_e^2 \lambda^2 \overline{(\Delta N)^2}\, LD \sec\chi \; \frac{1 + 0.5\,(h \sec\chi/Z)^2}{1 + (h \sec\chi/Z)^2} \qquad (2.60)$$

$$\overline{(AA/A)^2} = 4\, r_e^2 \lambda^2 \overline{(\Delta N)^2}\, LD \sec\chi \; \frac{0.5\,(h \sec\chi/Z)^2}{1 + (h \sec\chi/Z)^2} \qquad (2.61)$$

when $h \sec\chi) > Z$

$$\overline{(\Delta\phi)^2} = \overline{(\Delta A/A)^2} = 2\, r_e^2 \lambda^2 \overline{(\Delta N)^2}\, LD \sec\chi \qquad (2.62)$$

when $h \sec\chi << Z$

$$\overline{(\Delta\phi)^2} = 4\, r_e^2 \lambda^2 \overline{(\Delta N)^2}\, LD \sec\chi \qquad (2s63)$$

$$\overline{(\Delta A/A)^2} = \frac{2}{\pi^2}\, r_e^2 \lambda^4 \overline{(\Delta N)^2}\, \frac{h^2}{L^3}\, D \sec^3\chi \qquad (2.64)$$

These relations are said to explain weak mid-latitude scintillation for parameters in the order of L = 800 m (scale size of Fig. 2.14), D = 200 km (thickness of ionosphere), and h = 300 km (height to center of ionosphere). In the analysis outlined above, a layer of substantial thickness is considered, but in other treatments the layer is replaced by an equivalent two-dimensional screen, Thus scintillation may be discussed in terms of a diffracting screen model (Cronyn, 1970). For present purposes, we will not distinguish between scattering by a layer or a screen,

For the theory of weak scattering to apply, it has been assumed that the phase variation introduced by the ionosphere is restricted to about 1 radian. For this condition, the amplitude variations

observed at the ground are considered to correspond to the pattern of irregularities in the ionosphere, for irregularities below a certain size. If the phase variation is greater than 1 radian, the correspondence breaks down (Lawrence, Little, and Chivers, 1974). The amplitude scintillation index tends to increase with distance below the ionospheric layer but remains less than unity for weak scattering. The amplitude scintillation index for strong scattering can reach a value of unity and saturate or limit at that value, whereas phase scintillation does not reach a saturation point but continues to increase if the intensity of scattering continues to increase. An analysis by Rino and Fremouw (1977) indicated that phase variations are commonly in excess of 1 radian even when amplitude scintillation is weak.

The total field intensity at the ground is the sum of an unperturbed component and the perturbations in field intensity due to irregularities as in Fig, 2.15, The generation of perturbations can be understood in terms of electrical currents that flow in the irregularities due to the incident field intensity. Because of these currents, having a density different than that of the surrounding ionosphere, the irregularities act like antennas having rughly conical radiation patterns as suggested in Fig. 2.14. The beamwidth of the conical beams is about λ/L, the larger the irregularity the narrower the beamwidth and vice versa. At an observing point at a distance d below the layer where $d < (z = L^2$, with z the Fresnel distance corresponding to the scale length L, only one beam is intercepted and only phase variations are recorded. For larger distances, the cones of radiation overlap and conditions for interference and consequent amplitude scintillations occur.

Assuming weak scattering and a pattern of ionospheric irregularities drifting horizontally, the above discussion indicates qualitatively how amplitude scintillations develop. A further question, however, is under what conditions will the amplitude scintillations correspond to and allow determination of the sizes of the irregularities. An additional requirement, if this condition is to be met, is that, as mentioned above, the irregularities must not be too large. In particular, the irregularities must not fill more than the first Fresnel zone. Radiation from the even Fresnel zones interferes with that from the odd zones (Appendix 2.1) and this condition introduces effects

that preclude the identification of irregularities having scale sizes larger than $(\lambda z)^{1/2}$ [Eq. (2.52b)]. Phase scintillations, however, are not so limited and can be used to detect irregularities over a large range of scale sizes. Also they do not saturate but cover a wide dynamic range.

The temporal and spatial fluctuations of phase and amplitude are related to the power spectrum and autocorrelation function of electron density variations, the power spectrum and autocorrelation function being Fourier transforms of each other (Beckmann, 1957). Early analyses assumed a Gaussian form for the power spectrum (Briggs, and Parkin, 1963), but Rufenach (1972) assumed a power-law form. The relation between irregularity size l_x and the corresponding frequency of temporal phase variation depends on the velocity of the moving pattern of irregularities. Assuming the pattern to be moving in the x direction with velocity v_x, $l_x = v_x T = v_x/f$ and $f = v_x/l_x$. The frequency f is that of the temporal variation in signal phase corresponding to a periodicity in electron density of l_x, and T is the period of the temporal variation. The vector velocity of the moving pattern of irregularities can be determined by the use of three spaced antennas when the direction of the velocity is originally unknown (Coles, 1978),

The model involving diffraction in an ionospheric screen or layer has been widely employed to analyze scintillation, but it has been asserted that it may not be suitable if the irregularities are not confined to a sufficiently thin layer and if amplitude variations already occur at the lower boundary of the layer. First-order perturbation solutions of the scalar wave equation, based on the Rytov approximation or the method of smooth perturbations presented by Tatarski (1967,1971) are said to provide a means of treating the general case (Jokipii, '1973; Woo and Ishimaru, 1973, 1974; Crane, 1977; Ishimaru, 1978). The diffracting screen or layer model has been defended as being convenient and accurate for treating ionospheric scintillation (Bramley, 1977) and has been used by Rino (1979a,b) in his analysis of scintillation. Some proponents of the Rytov approximation say that the diffracting screen model gives good results in some cases but not in others, whereas the Rytov approximation is applicable generally. Some proponents of

the diffracting screen model say that it gives good results, that it involves concepts equivalent to the use of a lumped-constant equivalent circuit for treating transmission problems, and that the Rytov approximation does not always correctly predict observed scintillation characteristics.

2.6.2 Effect of Source Size, Interplanetary Scintillations

Star twinkle in visible light but, because of their larger angular size, planets do not. The same effect of size occurs for radio waves. The reduction in scintillation when the source has an angular width greater than a certain value is due to the fact that the diffraction pattern on the ground is the convolution of the point-source pattern and the "brightness distribution of the source. For weak scattering, the angular width of the source $\Delta\theta$ must be less than the angular width of the irregularities as seen from the ground if scintillation is to develop. The relation used by Lawrence, Little, and Chivers (1964) is that

$$\Delta\theta \lesssim L/2\pi d \tag{2.70}$$

for scintillation to occur, where L is the scale size of the irregularities and d is the distance to the irregularities. For strong scattering, they take

$$\Delta\theta < L/2\pi d\phi \tag{2.71}$$

for scintillation to be evident, where ϕ is the magnitude of the average phase change in radians and is greater than 1 radian. The effect of source size was recognized by Briggs (1961). Typically, radio sources must be smaller than about 6 to 10 minutes of arc if ionospheric scintillation is to develop.

In recording signals from radio sources of very small size along paths passing close to the Sun, Hewish, Scott, and Wills (1964) observed scintillations having short periods, typically around 1 s, which is small compared with the periods, typically around 30 s, that had been associated with ionospheric scintillations up to that time. For such short-period scintillations to be recorded, the sources must have angular widths of about 0.5 second or arc or less. (The angular extent of sources can be determined by interferometry techniques.) On the basis of the relations embodied

in Eqs (2 7.0) and (2 7.1) and taking into account that the signa paths passed through the solar wind close to the Sun., it was concluded that the scintillations were of interplanetary origin. An account of the early observations of interplanetary scintillation (IPS) has been provided by Cohen (1969). The use of IPS has become an important means for obtaining information about the solar wind (Woo, 1975,1977).

Before IPS were recognized, it was noted that radio-star signals that passed near the Sun experienced angular broadening (Hewish, 1955). What was actually observed was a decrease in signal amplitude. This decrease could not be explained on the basis of absorption or refraction but only on the basis of angular broadening due to scattering by electron density irregularities. Angular broadening has been vividly illustrated as such by two-dimensional displays produced by a radio heliograph operating at 80 MHz (Blessing and Dennison, 1972). The radiohel iograph, having a beamwidth at the zenith of 3.9 rein, produces a 2 deg square-area picture of the sky every second.

When Pioneer 6, having a stable monochromatic signal was occulted by the Sun, another effect, spectral broadening, was observed (Goldstein, 1969). To record spectral broadening, the sidebands of the spacecraft signal are eliminated by filtering and only the pure carrier is recorded. Spectral broadening causes the carrier which originally has an exceedingly narrow width in frequency to be broadened in frequency. The phenomena may be caused by the Doppler shift of elements of radiation that are scattered from electron density irregularities or by amplitude scintillation orbya combination of both mechanisms.

2.6.4 Observed Characteristics of Scintillation

Scintillation tends to be most intense in equatorial, auroral, and polar latitudes and to have a general pattern of occurrence as shown in Fig. 2.13 (Aarons, Whitney, and' Allen, 1971; CCIR, 1986 b). Table 2.3 gives examples of observed percentages of occurrence of scintillation at frequencies of 137 and 254 MHz. The table includes K_p values, which are measures of magnetic activity, and shows that scintillation increases with K_p at sub-amoral and auroral latitudes.

The unexpected occurrence of scintillation at microwave frequencies at equatorial latitudes is illustrated for 6 GHz in Fig. 2.16 by Taur (1973), who presented further examples of the same type. Equatorial scintillation is often characterized by a sudden onset, and its occurrence varies considerably with location within the equatorial region. Basu et al. (1980) obtained data at 1.54 GHz at Huancayo, Peru for a 20-month period in 1976-1977 using the MARISAT satellite. Scintillation generally occurs after sunset and before midnight, with maximum intensities in roughly Feb.-March and Sept.-Ott. (Fig.2. 17). Aarons et al, (1981a) obtained data at 1.54 GHz during the peak of the sunspot cycle in 1979 and 1980 from Huancayo; Natal, Brazil; and Ascension Island, Peak-to-peak fading greater than 27 dB was recorded at Ascension Island, and 7-9 dB were recorded at Huancayo and Natal. The latter two locations are close to the magnetic equator in what in knownas the electrojet region. Ascension Island is at approximately 17 deg S dip latitude and is in the equatorial anomaly, namely the region from about 15 to 20 deg north and south of the magnetic dip equator where electron densities are higher than at the geomagnetic equator itself (Rishbeth and Garriot, 1969). Additional information about scintillation in the equatorial anomaly has been presented by Mullen et al. (1985). Scintillation greater than 30 dB at 1.5 GHz and 7 dB at 4 GHz was observed. Fan and Liu (1983) describe studies of GHz equatorial scintillations in the Asian region. Peak-to-peak fluctuations up to 14 dB were recorded. Aarons (1985) and Fanke and Liu (1985) have modeled equatorial scintillation, with particular attention given to observations at Huancayo and Ascension Island, respectively.

Mid-latitude scintillation shows a well-established maximum near midnight, corresponding to the occurrence of spread F.

Table 2.3 Percentage of occurrence of scintillation (CCIR, 1982, 1986b). (a) ≥ 10 dB peak to peak, equatorial latitudes

Location	Frequency	Day	Night
		(400-1600 LT)	(1600-400 LT)
Huancayo, Peru	137 MHz	3	14
	254 MHz	2	7
		(600-1800 LT)	(1800-600 LT)
Accra, Ghana	137 MHz	0,4	14

(b) ≥ 12 dB peak to peak at 137 MHz, subauroral and auroral lat.

Location	K_p	Day (500-1700 LT)	Night (1700-500 LT)
Sagamore Hill, MA	O to 3+	o	1.4
	> 3+	0.1	2
Goose Bay, Labrador	O to 3+	0.1	1.8
	> 3+	1.6	5.8
Narssarssuaq, Greenl.	O to 3+	2.9	18
		19	45

(c) ≥ 10 dB peak to peak at 254 MHz, auroral latitudes

Location	K_p	Day (600-1800 LT)	Night (1800-600 LT)
Goose Bay, Labrador	O to 3+	0.1	0.1
	> 3+	0.3	1.2
Narssarssuaq, Greenl.	O to 3+	0.1	0.9
		2.6	8.4

LT: Local Time

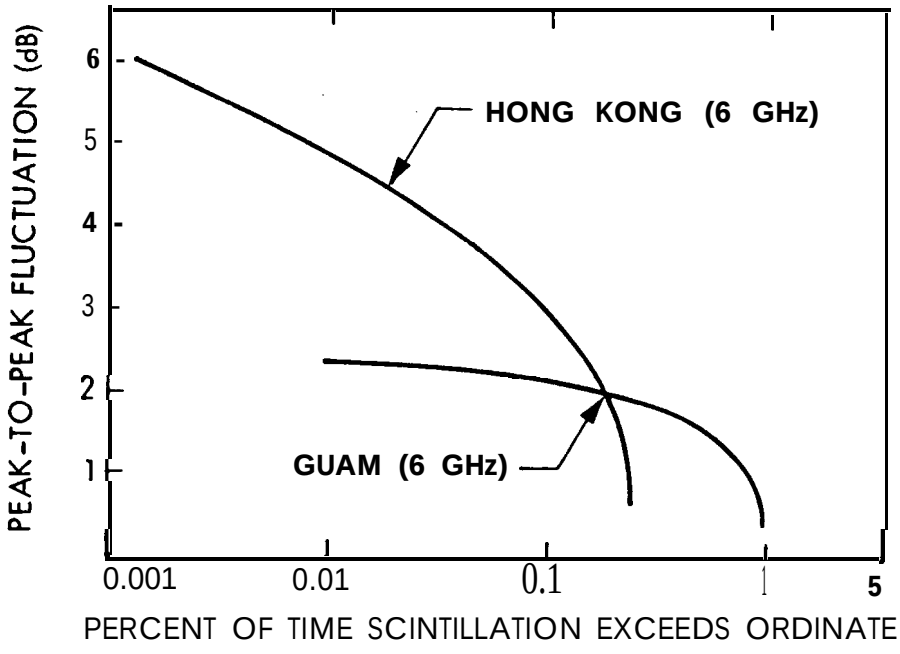

Figure 2.16. Scintillation, Guam and Hong Kong (Taur, 1973).

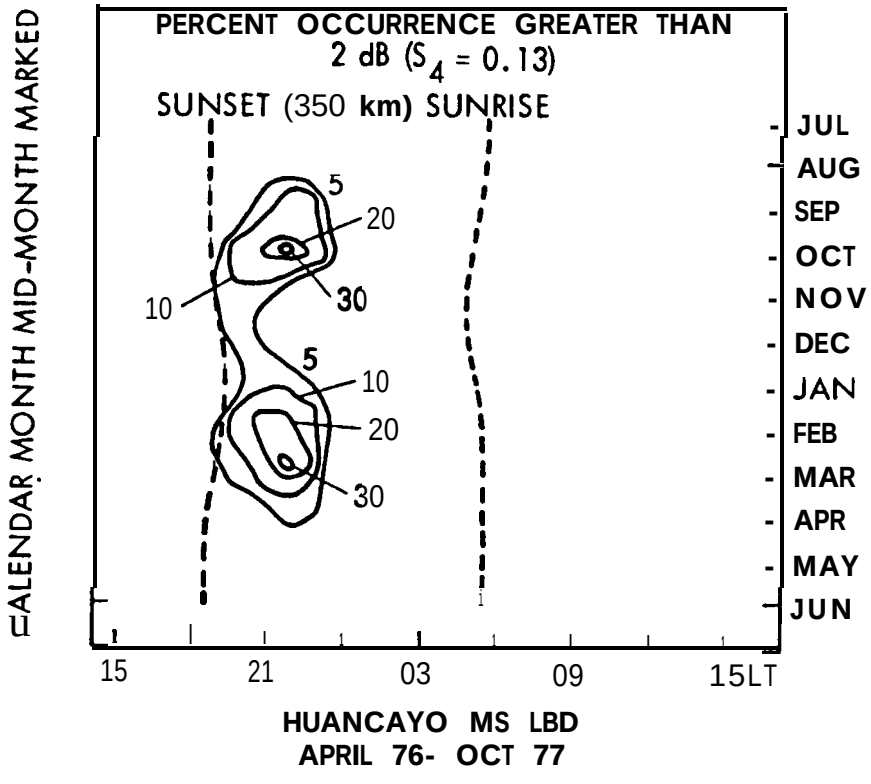

Figure 2.17. Monthly percentage of scintillations ≥ 2 dB, Huancayo, MARISAT, 1.54 GHz, (Basu et al., 1980).

Scintillation at middle latitudes is generally not intense, but some cases of severe scintillation have been recorded in Japan. During a magnetic storm on March 27, 1979, peak-to-peak scintillation of 18, 10, 15, and 3.5 dB were recorded at 136 MHz and 1.7, 4, and 12 GHz, respectively, on different paths in and around Japan (Minakoshi et al. 198 1). Another report from Japan of severe scintillation, in this case of 1,5 GHz signals, has been provided by Karasawa et al. (1985). Signals from a MARISAT satellite over the Indian Ocean at an elevation angle of 17.3 deg were utilized. Fluctuations lasting for a long period and sometimes exceeding 30 dB peak-to-peak in the equinoctial month were observed and shorter spike-like scintillations were also evident.

Scintillation increases at high latitudes, the increase beginning near the region of the ionospheric trough. In the auroral oval, both discrete and diffuse aurora, as shown by Defense Meteorological Satellite images, have been correlated with scintillation at 136-137 MHz (Martin and Aarons, 1977). Frihagen (197 1), using 40 MHz transmissions, has reported two regions of peak scintillation activity at high latitudes, one corresponding to the au-oral oval and one above 80 deg geomagnetic latitude over the polar cap. Aarons et al. (198 1 b) have prepared plots showing percentages of occurrence of scintillation greater than 10 dB in the polar cap at Thule, Greenland at a frequency of 250 MHz. Buchau et al. (1985) relate 250-MHz scintillation to ionospheric structures in the polar cap. S. Basu et al. (1985) report the first long-term measurements of phase scintillations at high latitude at 250 MHz. The median and 90th percentile values of rms phase deviation at 250 MHz for an 82 second detrend interval are 2 and 6 rad, respectively, at both auroral and polar cap locations.

Measurements by Fremouw et al. (1978) employing 10 frequencies between 137 and 2891 MHz transmitted from a satellite in a high-inclination orbit and recorded at equatorial and auroral latitudes (Anton, Peru; Kwajalein Island; and Fairbanks, Alaska) showed an $f^{-1.5}$ variation of the intensity of amplitude scintillations with frequency for S_4 less than 0.4 and an f^{-1} variation of phase scintillation with frequency. The more recent HiLat mission, utilizing satellite P83-1 with a 10-frequency radio

beacon, had the objective of obtaining quantitative information on the spatial and temporal spectra of high-latitude amplitude and phase scintillation. The satellite was launched on June 27, 1983 from Vandenberg Air Force base. Early results of this mission have been presented by Fremouw et al. (1985).

Amplitude scintillations result in reduction of signal-to-noise ratio for a fraction of the time, Phase scintillations may or may not be important depending on the type of system. For digital systems, phase scintillations may be unimportant if the bit rate is much greater than the scintillation rate. Phase scintillations tend to, be important for radio navigation systems such as GPS and for synthetic-aperture radars. For positioning systems phase scintillation results in range jitter and consequent loss of precision in range (Rino, Gonzalez, and Hessing, 1981; Yeh and Liu, 1979) as increments of phase $\Delta\phi$ and corresponding changes in apparent range $AR_{@}$, are related by $\Delta\phi = (2\pi/\lambda_o)\,\Delta R_\phi$ [Eq. (2.46)]. Loss of signal coherence is another possible effect from scintillation (Rino, Gonzalez, and Hessing, 198 1). Loss of coherence across a band as narrow as 11.5 MHz at UHF was observed by Fremouw et al. (1978).

Amplitude scintillations can be described by use of power spectra, autocorrelation functions, cumulative probability distributions, fade-duration distributions, and plots showing message reliability (Whitney and Basu, 1977). Power spectra have been presented by a number of authors including Rufenach (1972), Crane (1976), and Whitney and Basu (1977). Examples of power spectra are shown in Figs. 2.18. Cumulative probability distributions show the percentage of time that signal amplitude exceeds specified dB values. The Nakagami-m distribution shows good agreement with observed distributions (Whitney and Basu, 1977; Fremouw et al., 1978; Panter, 1972). For the m of this distribution equal to unity (not to be confused with the scintillation index m), the distribution is a Rayleigh distribution.

The power spectra, cumulative probability distributions, etc. contain detailed information about scintillation characteristics, but frequently one is primarily interested in certain parameters such as

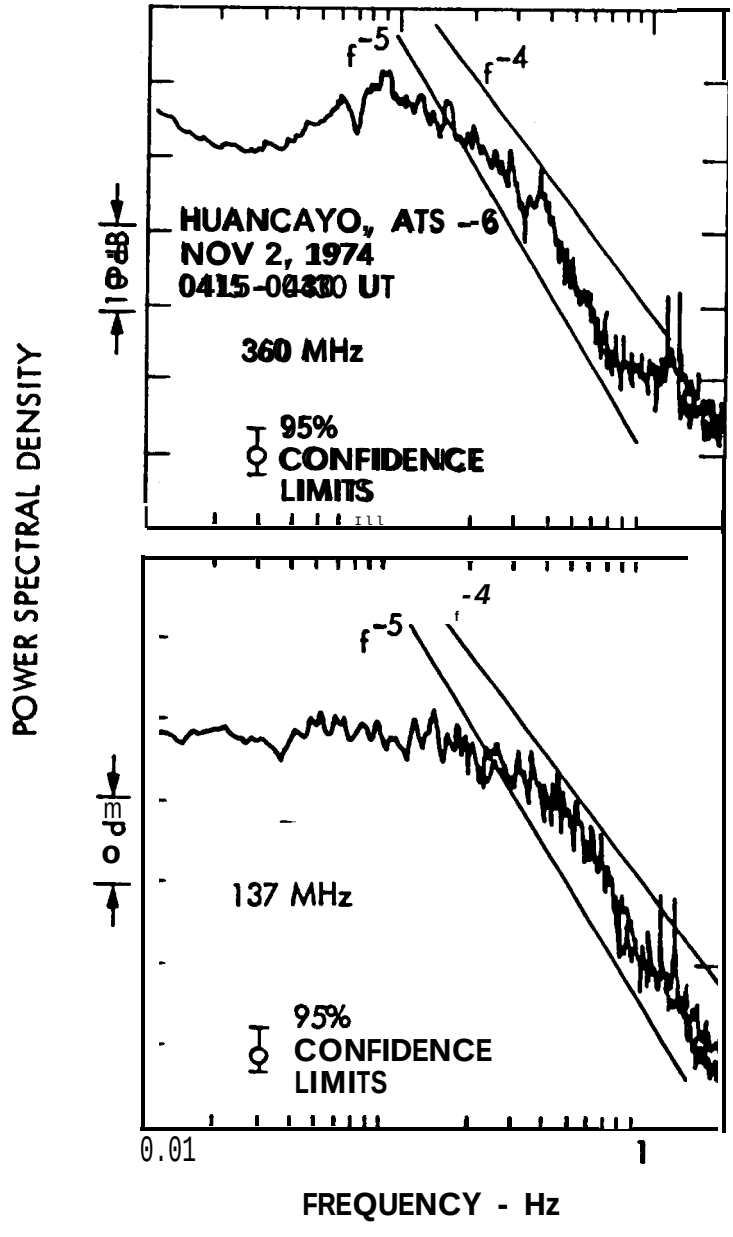

Figure 2.18. Typical power -spectra for intense scintillations; S_4 = 0.78 at 360 MHz, S_4 = 0.94 at 137 MHz (Whitney and Basu, 1977).

mean value, standard deviation, scintillation index, and coherence time. The index S_4 is the ratio of standard deviation to mean value. Coherence time τ_c can be obtained from plots of the autocorrelation function and is the time for this function to decrease from unity to some specified value such as 0.5 or 1/e. Whitney and Basu (1977) used 0.5 in their analysis of scintillation data. For predicting bit error rate, the form of the probability distribution function is needed.

In CCIR Report 263-6, values of the fading period of scintillation are given (CCIR, 1986b). The period varies over a large range and can be as long as several minutes. The fading period of GHz scintillation varies from 2 to 15 seconds.

2.7 ABSORPTION

Attenuation was not included in discussing the characteristic waves and Faraday rotation in previous sections, but waves propagating in the ionosphere experience dissipative attenuation which becomes increasingly important with decreasing frequency. A principal mechanism of attenuation is collisions of free electrons with neutral atoms and molecules. An electromagnetic wave propagating in a plasma imparts an ordered component of velocity to the electrons but the electrons lose some of the associated energy in the collision process. Hence the electromagnetic wave is attenuated. The attenuation coefficient α, determining the rate of decrease of electric field intensity with distance in accordance with $e^{-\alpha z}$ for the left circularly polarized wave, is given, using conventional magneto-ionic theory, by

$$\alpha_l = \frac{Nq^2 u}{2m\epsilon_o n_r c\,[(\omega + \omega_B)^2 + v^2]} \quad \text{Nepers/m} \qquad (2.72)$$

where v is the collision frequency. For the right circularly polarized wave, the corresponding expression is

$$\alpha_r = \frac{Nq^2 u}{2m\epsilon_o n_r c\,[(\omega - \omega_B)^2 + v^2]} \quad \text{Nepers/m} \qquad (2.73)$$

All quantities are in S1 units. N is in electrons/m^3 ; q, the electron charge, equals 1.6022 $\times 10^{-19}$ C; m = 9.1096 $\times 10^{-31}$ kg; ϵ_o = 8.854 x 10^{-12} F/m; n_r is the real part of the index of refraction; c = 2.9979 x 10^8 m/s; $\omega = 2\pi f$ with f in Hz; and v is collision frequency in Hz. When attenuation is taken into account, the index of refraction becomes complex and is a function of collision frequency as well as electron density. The value of the real part n_r can be calculated precisely, based on assumed values of N and u, but if losses are slight n_r has essentially the same value as for the lossless case, for which n = n_r and is entirely real. Note that ω appears in the denominator and that for $\omega >> \omega_B$, where ω_B is angular gyrofrequency, and ω)> u, attenuation varies inversely with ω^2. The frequencies used for space communication are generally sufficiently high that attenuation does vary inversely with frequency squared and n_r does have the same value as in the lossless case. Also, n_r approaches unity as frequency increases.

For frequencies above about 30 MHz or for transverse propagation of the ordinary wave, the attenuation constant varies inversely with frequency squared and takes the simpler form

$$a = \frac{Nq^2 v}{2m\epsilon_o n_r c\, \omega^2} \quad \text{Nepers/m} \qquad (2.74)$$

To obtain attenuation in dB/m, the value of α in Nepers/m can be multiplied by 8.686.

For oblique paths, total attenuation is proportional to $\sec\chi/f^2$, where χ is the zenith angle, for frequencies above 30 MHz (CCIR, 1986b). Attenuation tends to be low at the frequencies used for space communications, the highest attenuations occurring under conditions of auroral and polar-cap absorption,

Table 2.4 shows values of auroral absorption at a frequency of 127 MHz as published in CCIR Report 263-6 (CCIR, 1986b), In a typical night of auroral activity at Fairbanks, Alaska, long quiet auroral arcs appear to the north before midnight. These progress southward and may reach close to the zenith by 23 h local time. One or two westward traveling folds or surges in the otherwise quiet arcs may have been observed by this time. Between 23 h and 02 h the auroral forms become widespread and active in the sky, this phase being known as the auroral breakup. After the breakup, patchy, luminous forms appear in the sky. Quiet arcs may then reappear as the opening phase of a second cycle of activity. Auroral absorption is usually greatest in the breakup and post-breakup periods.

Figure 2.19 shows illustrative hypothetical plots of absorption during a polar-cap absorption event at 30 MHz, as could be derived from riometer events. The top curve applies in the summer when sunlight occurs for 24 hours a day. The other two curves for equal periods of day and night show a pronounced diurnal variation in absorption. The decrease in absorption at night is due to the decreased density of free electrons that occurs when solar radiation is absent,

Table 2.4 Auroral Absorption at 127 MHz, dB (CCIR, 1986b).

Percentage of time	Elevation Angle	
	20°	5°
0.1	1.5	2.9
1	0.9	1.7
2	0.7	1.4
5	0.6	1.1
50	0.2	0.4

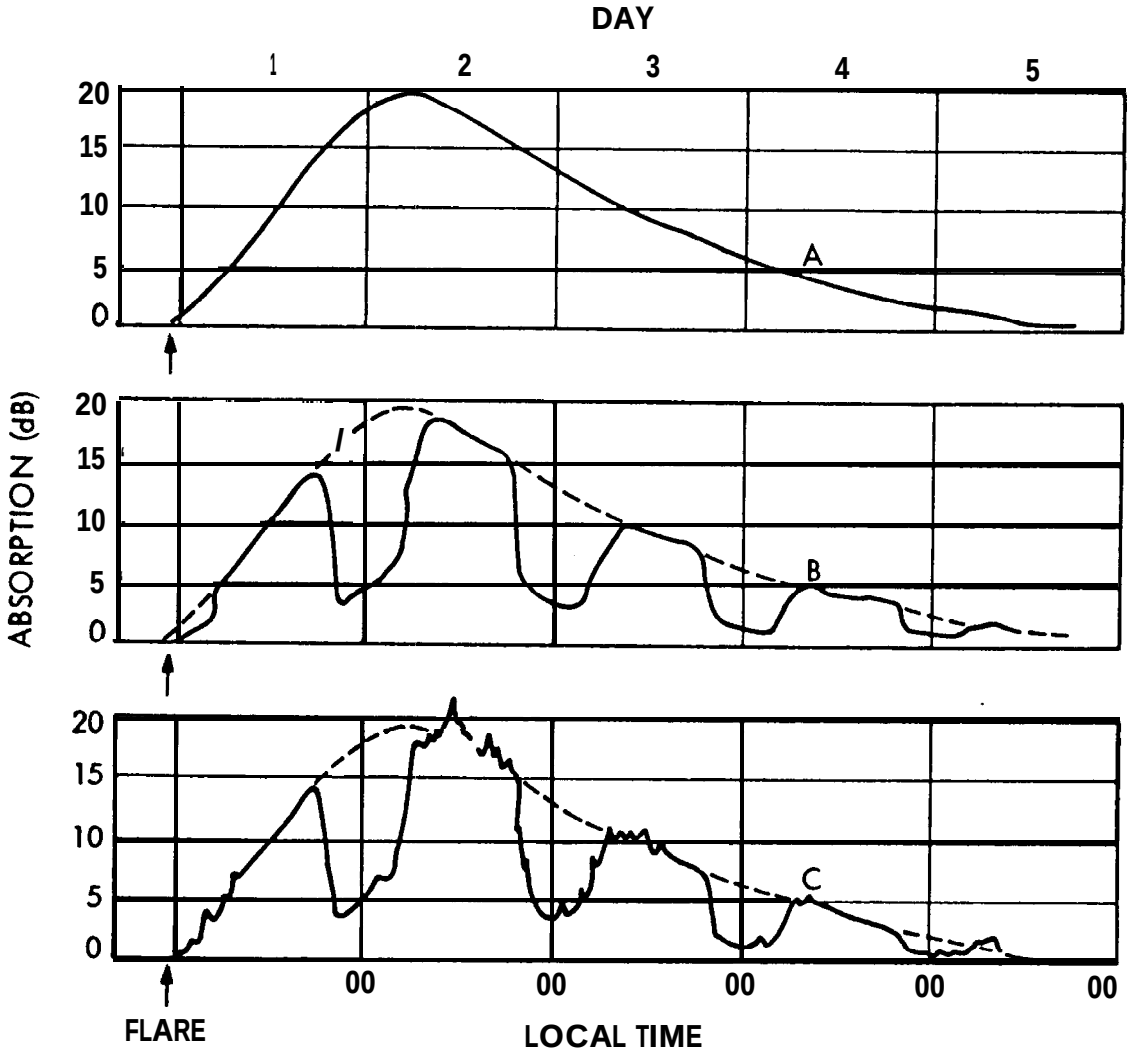

Figure 2.19. Hypothetical model showing polar cap absorption following a major solar flare as expected to be observed on riometers at approximately 30 MHz. (CCIR, 1986 b).

A: High latitudes, 24 h of daylight.
B: High latitudes, equal day and night.
C: Auroral zone.

2.8 TRANSIONOSPHERIC PROPAGATION PREDICTIONS AND CORRECTIONS

For some satellite systems advance estimates of ionospheric parameters in the planning stage are sufficient, but for other systems continuous y updated long-term (e.g. monthly) or short-term (e.g. daily) predictions may be needed. Furthermore, real-time or near-real-time values of ionospheric parameters may be required in some cases.

The problem of ionospheric predictions was considered in a conference devoted to solar-terrestrial predictions (Donnelly, 1978). Included in the proceedings of the conference is a report treating transionospheric propagation predictions (Klobuchar and Working Group, 1978). It is stated in the working group report that monthly values of TEC can probably be predicted within ±20 percent for regions where a time history of TEC exists. However, even if monthly mean values could be predicted perfectly accurately, short-term variations from the monthly mean values would still present a problem. Much of the difficulty arises from the ionospheric effects of geomagnetic storms. Theretical capabilities were not considered to be capable of predicting storm-related TEC behavior, and prediction procedures based on morphological data are the only alternative. The report discusses the problem and possible remedies.

Faraday-rotation data from linearly plarized 137-MHz beacons of the geostationary satellites ATS-1, SIRIO, and Kiku-2 have been used by the Jet Propulsion Laboratory to measure TEC and determine ionospheric corrections to range and Doppler data used for Voyager spacecraft navigation (Royden et al., 1980). By taking the difference between TEC values determined by Faraday rotation and TEC values from dual-frequency transmissions from Voyager (2295 MHz in the S band and 8415 MHz in the X band), the electron content of the path beyond the ionosphere is also determined. The electron content beyond the ionosphere includes that of the plasmasphere and the solar plasma. In passing by the moon Io of Jupiter, electrons in its atmosphere contributed to the total electron content along the path and made possible a comparison of

experimental results and theoretical models of the electron density surrounding Io. A two-frequency technique involving time-delay measurements for determining TEC, in order to correct for its effects, was described in Sec. 2.3.1.

In addition to the periodical literature, URSI (International Scientific Radio Union), the CCIR (International Radio Consultative Committee), and the series of Ionospheric Effects Symposia are good sources of information about the ionosphere and its effects. U.S. Commission G, Ionospheric Radio and Propagation of URSI, usually participates in two URSI meetings per year in the United States, and URSI holds international General Assemblies every three years. Volume VI of Recommendations and Reports of the CCIR and the CCIR working groups which cent ribute to it treat Propagation in Ionized Media. The fifth Ionospheric Effects Symposium (IES) was held in May, 1987 in Springfield, Virginia, sponsored by the Naval Research Laboratory, the Office of Naval Research, the Air Force Geophysics Laboratory, and the Army Center for Communications. The May/June 1985 issue of Radio Science was devoted to papers presented at the 1984 IES, and several of these are cited in this chapter.

REFERENCES

Aarons, J., J.P. Whitney, and R.S. Allen, "Global morphology of ionospheric scintillations," Proc. IEEE, vol. 59, pp. 159-172, Feb. 1971,

Aarons, J. et al., "Microwave equatorial scintillation intensity during solar maximum," Radio Sci., vol. 10, pp. 939-945, Sept.-Ott. 198 la.

Aarons, J. et al., "VHF scintillation activity over polar latitudes," Geophys. Res. Lett., vol. 8, pp.277-280,1981b.

Aarons, J., "Construction of a model of equatorial scintillation intensity," Radio Sci., vol. 20, pp. 397-402, May-June 1985.

Akasofu, S. I., Polar and Magnetospheric Subsystems. New York: Springer-Verlag, 1968.

Balsley, B. B., "Some characteristics of non-two-stream irregularities in the equatorial electrojet," J. Geophys. Res., vol. 74, pp2333 -2347, May 1, 1969.

Baron, M. J., "Electron densities within aurorae and other auroral E-region characteristics," Radio Sci., vol. 9, pp.34 1-348, Feb. 1974.

Basu, S. et al., "Long-term 1.5 GHz amplitude scintillation measurements at the magnetic equator," Geophys. Res. Lett., vol. 7, pp. 259-262, April 1980.

Basu, S. et al., Morphology of phase and intensity scintillations in the auroral oval and polar cap," Radio Sci., vol.20, pp. 347-356, May-June1985.

Beckmann, P. Probability in Communication Engineering. New York: Harcourt, Brace, and World, 1967.

Blesing, R.G. and P.A. Dennison, "Coronal broadening of the Crab Nebula 1969-1971: observations," Proc. Astron. Sot. Australia, vol.2, pp. 84-86, March 1972.

Booker, H. G., "The role of the magnetosphere in satellite and radio-star scintillation," J. Atmos. Terr. Phys., vol. 37, pp. 1089-1098, Aug. 1975.

Booker, H. G., "The role of acoustic gravity waves in the generation of spread-F and ionospheric scintillation," J. Atmos. Terr. Phys., vol. 41, pp. 501-515, May 1979.

Bowhill, S. A., "Statistics of a radio wave diffracted by a random ionosphere," J. of Research of NBS, vol. 65D, pp. 275-292, May-June1961.

Bramley, E. N., "The accuracy of computing ionospheric radio-wave scintillation by the thin-phase-semen approximation," J. Atmos. Terr. Phys., vol.39, pp. 367-373, March 1977.

Briggs, B. H., "The correlation of radio star scintillations with geomagnetic disturbances," Geophysical J., vol. 5, pp. 306-317, Oct. 1961.

Briggs, B.H. and I.A. Parkin, "On the variation of radio star and satellite scintillation with zenith angle," J. Atmos. Terr. Phys., vol. 25, pp. 339-365, June 1 963,

Buchau, J. et al., "Ionospheric structures in the polar cap: their origin and relation to 250-MHz scintillation," Radio Sci., vol, 20, pp. 325-338, May-June 1985.

Budden, K. G., Radio Waves in the Ionosphere. Cambridge: Cambridge U. Press, 1961.

Callahan, P.S., "Columnar content measurements of the solar-wind turbulence near the sun," Astrophys. J., vol. 199, pp. 227-236, July 1, 1975.

CCIR, Report 263-5, 1982. [Earlier version of CCIR, 1986 b.]

CCIR, Report 565-3, "Propagation data for broadcasting from satellites," in Volume V. Propagation in Non-ionized Media, Recommendations and Reports of the CCIR, 1986. Geneva: Int. Telecomm. Union, 1986a.

CCIR, Report 263-6, "Ionospheric effects upon earth-space propagation," in Volume VI. Propagation in Ionized Media, Recommendations and Reports of the CCIR, 1986. Geneva: Int. Telecomm. Union, 1986b.

Cohen, M. H., "High-resolution observations of radio sources," Annual Rev. of Astron. and Astrophys., vol. 7, pp. 619-664, 1969.

Coles, W. A., "Interplanetary scintillations," Space Sci. Rev., vol 21, pp. 411-42?, 1978.

Craft, H.D. and L.H. Westerlund, "Scintillation at 4 and 6 GHz caused by the ionosphere," 10th Aerospace Sci. Meeting, AIAA Paper No. 72-179, 1972.

Crain, C. M., H.G. Booker, and J.A. Ferguson, "Use of refractive scattering to explain SHF scintillations," Radio Sci., vol. 14 pp. 125-134, Jan. -Feb. 1979.

Crane, R. K., "Spectra of ionospheric scintillation," J, Geophys Res., vol. 81, pp. 2041 -20S0, May 1, 1976.

Crane, R. K., "Ionospheric scintillation," Proc. IEEE, vol. 65, pp. 180-199, Feb. 1977.

CRC (Weast, R.C. cd,), Handbook of Chemistry and Physics, 52nd Edition, p. F189. Cleveland, OH: Chemical Rubber Co., 1972.

Cronyn, W. M., "The analysis of radio scattering and space-probe observations of small-scale structure in the interplanetary medium," Astrophys. J., vol. 161, pp. 755-763, Aug. 1970.

Davies, K., Ionospheric Radio Propagation. Washington, DC: Supt. of Documents. U.S. Government Printing Office, 1965.

Davies, K., Ionospheric Radio Waves, Waltham, MA: Blaisdell Pub. Co., 1969.

Davies K., G. K.. Hartmam, and R. Leitinger, "A comparison of several methods for estimating columnar electron content of the plasmasphere," J. Atmos. Terr. Phys., vol. 39, pp. 571-580, May, 1977.

Davies, K., "Recent progress in satellite radio beacon studies with particular emphasis on the ATS-6 radio beacon experiment," Space Sci. Rev., vol. 25, pp. 357-430, April 1980.

Donnelly, R. F. (cd.), Solar Terrestrial Predictions Proceedings, Volumes 1-4. Boulder, CO: Environ. Res. Labs., NOAA, 1978.

Evans, J. V., "Theory and practice of ionospheric study by Thomson scatter radar," Proc. IEEE, vol. 57, pp. 496-530, April 1969.

Fang, D.J. and C.H. Liu, "A morphological study of gigahertz scintillation in the Asian region," Radio Sci., vol. 18, pp. 241-252, 1983.

Farley, D. T., "A plasma instability resulting in field-aligned irregularities in the ionosphere," J. Geophys. Res., vol. 68, pp. 6083-6097, Nov. 15, 1963.

Feldstein, Y. I., "A quarter of a century with the auroral oval," EOS, vol. 67, Oct. 7, 1986.

Flock, W.L., Electromagnetics and the Environment: Remote Sensing and Telecommunications. Englewood Cliffs, NJ: Prentice-Hall, 1979.

Franke, S.J. and C.H. Liu, "Modeling of equatorial multifrequency scintillation," Radio Sci., vol. 20, pp. 403-415. May-June, 1985.

Fremouw, E. J., et al., "Early results from the DNA wideband satellite experiment - complex signal scintillation," Radio Sci., vol. 13, pp. 167-187, Jan. -Feb. 1978.

Fremouw, E. J., et al., "The HiLat satellite mission," Radio Sci., vol. 20, pp. 416-424, May-June 1985.

Frihagen, J.9 "Occurrence of high latitude ionospheric irregularities giving rise to satellite scintillation." J. Atmos. Terr. Phys., vol. 33, pp. 21-30, 1971.

Goldstein, R. M., "Superior conjunction of Pioneer 6," Science, vol. 166, pp. 598-601, 31 Oct. 1969.

Hawkins, G.S. and J.A. Klobuchar, "Seasonal and diurnal variations in the total electron content of the ionosphere a invariant latitude 54 degrees," AFCRL-TR-74-0294. Bedford, MA: Air Force Carob. Res. Labs., 28 June 1974.

f-lay, J. S., S.J. Parsons, and J. W. Phillips, "Fluctuations in cosmic radiation at radio frequencies," Nature, vol. 158, p. 234, Aug. 17, 1946.

Heron, M. L., "Transequatorial propagation through equatorial plasma bubbles - discrete events," Radio Sci., vol. 15, pp. 829-835, July-Aug. 1980.

Hewish, A., "The diffraction of galactic radio waves as a method of investigating the irregular structure of the ionosphere," Proc. Royal Soc. of London, Series A, vol. 214, pp. 494-514, 9 Oct. 1952.

Hewish, A., "The irregular structure of the outer regions of the solar corona," Proc. Royal Sot. of London, Series A, vol. 228, pp. 238-251, 22 Feb. 1955.

Hewish, A., P.F. Scott, and D. Wills, "Interplanetary scintillation of small diameter radio sources," Nature, vol. 203, pp. 1214-1217, Sept. 19, 1964.

Hines, C.O. et al., The Upper Atmosphere in Motion, Geophysical Monograph 18. Washington, DC: A. Geophys. Union, 1974.

HunSucker, R.D., "Simultaneous riometer and incoherent scatter radar observations of the auroral D region," Radio Sci., vol. 9, pp. 335-340, Feb. 1974.

Ishimaru, A., Wave Propagation and Scattering in Random Media, Vol. 2. New York: Academic Press, 1978

Jokipii, J. R., "Turbulence and scintillations "in the interplanetary plasma," Ann. Rev. of Astron. and Astrophys., vol. 11, pp. 1-28, 1973.

Karasawa, Y"., K. Yasukawa, and M. Yamada, "Ionospheric scintillation measurements at 1.5 GHz in mid-latitude region," Radio Sci., vol. 20, pp. 543-551, May-June 1985.

Kelso, J. M., Radio Ray Propagation in the Ionosphere. New York: McGraw-Hill, 1964.

Klobuchar, J. A., "Ionospheric effects on satellite navigation and air traffic control systems," in Recent Advances in Radio and Optical Propagation for Modem Communication, Navigation, and Detection Systems, AGARD Proceedings - LS-93, **ISBN** 92-835-1280-4. NTIS: Springfield, VA 22161, April 1978.

Klobuchar, J.A. (leader) and Working Group, "B. Trans-ionospheric propagation predictions," in R.F. Donnelly (cd.), vol. 2: Working Group Reports and Reviews of Solar-Terrestrial Predictions Proceedings, pp. 217-245, Boulder, CO: Environ. Labs., NOAA, 1978.

Lawrence, R. S., C.G. Little, and H.J.A. Chivers, "A survey of ionospheric effects upon earth-space propagation," Proc. IEEE, vol. 52, pp. 4-47, Jan. 1964.

Leadabrand, R.L. et al., "Chatanika, Alaska auroral-zone incoherent scatter facility," Radio Sci., vol. 7, pp. 747-756. July 1972.

Little, C.G. and A.C.B. Lovell, "Origin of the fluctuations in the intensity of radio waves from galactic sources: Jodrell Bank observations," Nature, vol. 165, pp. 423-424, March 18, 1950.

Malin, S.R.C. and D.R. Barraclough, "An algorithm for synthesizing the geostationary field," Computers and Geosci., vol. 7, **No. 4,** pp. 401-405, 1981.

Martin, E. and J. Aarons, "F layer scintillations and the aurora," J. Geophys. Res., vol. 82, pp. 2717-2722, July 1, 1977.

McClure, J. P., W.B. Hanson, and J.H. Hoffman, "Plasma bubbles and irregularities in the equatorial ionosphere," J. Geophys. Res., vol. 82, pp. 2650-2656, July 1, 1977.

Millman, G.H. and G.M. Reinsmith, An analysis of the incoherent scatter-Faraday rotation technique for ionospheric propagation error correction," General Electric Tech. Inf. Series R 74 EMH2, Syracuse, NY, Feb. 1974.

Minakoshi, H. et al., "Severe ionospheric scintillation associated with magnetic storm on March 22, 1979," J. Radio Res. Labs. (Japan), vol. 28, pp. 1-9, 1981.

Mullen, J.P. et al., "UHF/GHz scintillation observed at Ascension Island from 1980 through 1982," Radio Sci., vol. 20, pp. 3S7-365, May-June 1985.

Panter, P. F., Communication Systems Design. New York: McGraw-Hill, 1972.

Peddie, N. W., "International geomagnetic reference field: the third generation," J of Geomag. and Geoelect., vol. 34, pp. 309-327, 1982.

Ratcliffe, J. A., An Introduction to the Ionosphere and Magnetosphere. Cambridge: Cambridge U. Press, 1972.

Rino, C.L., "A power law phase screen model for ionospheric scintillation, 1. Weak scatter," Radio Sci., vol. 14, pp. 1135-1145, Nov.-Dee. 1979a.

Rino, C. L., "A power law phase screen model for ionospheric scintillation, 2. Stron scatter, " Radio Sci., vol 14, pp. 1147-1155, Nov.-Dee. 1979%.

Rino, C.L. and E.J. Fremouw, "The angle dependence of singly scattered wave-fields," J. Atmos. Terr. Phys., vol. 39, pp. 859-868, Aug. 1977.

Rino, C. L., V.H. Gonzales, and A.R. Hessing, "Coherence bandwidth loss in transionospheric radio propagation," Radio Sci., vol. 16, pp. 245-255, March-April 1981.

Rishbeth, H. and O.K. Garriott, Introduction to Ionospheric Physics New York: Academic Press, 1969.

Royden, H. N., D. W. Green, and G.R. Walson, "Use of Faraday-rotation data from beacon satellites to determine ionospheric; corrections for interplanetary spacecraft navigation. " COSPAR/URSI Symposium on Scientific and Engineering Uses of Satellite Radio Beacons, Warsaw. Poland, May 19-23, 1980.

Rufenach, C. L., "Power-law wave number spectrum deduced from ionospheric scintillation observations, " J. Geophys. Res., vol. 77, p. 4761-4772, Sept. 1, 1982.

Smith, E.K., A Study of Ionospheric Scintillation as it Affects Satellite Communication, Office of Telecomm., U.S. Dept. of Commerce, Tech. Memorandum 74-186, Nov. 1974.

Smith, E.K. and R.E. Edelson, "Radio propagation through solar and other extraterrestrial ionized media," JPL Pub. 79-117. Pasadena, CA: Jet Propulsion Lab., Jan. 15, 1980.

Smith, F. G., "Origin of the fluctuations in the intensity of radio waves from galactic sources: Cambridge observations," Nature, vol. 165, pp. 422-423, March 18, 1950.

Tatarski, V. E., Wave Propagation in a Turbulent Medium. New York; McGraw-Hill, 1961.

Tatarski, V. E., The Effects of the Turbulent Atmosphere on Wave Propagation. Springfield, VA: National Technical Information Service, 1971.

Taur. R. R.. "Ionospheric scintillation at 4 and 6 GHz," COMSAT Tech. Rev., vol. 3, pp. 145-163, Spring 1973.

Whitney, H. E., J. Aarons, and C. Malik, "A proposed index "for measuring ionospheric scintillation," Planet. Space Sci., vol. 7, pp 1069-1073, 1969.

Whitney, H.E. and S. Basu, "The effect of ionospheric scintillation on VHF/UHF satellite communication," Radio Sci., vol. 12, pp. 123-133, Jan. -Feb. 1977.

Woo, R., "Multifrequency techniques for studying interplanetary scintillation," Astrophys. J., vol. 201, pp. 238-248, Oct. 1, 1975.

Woo, R. "Measurements of the solar wind using spacecraft radio scattering observations," in Study of Travelling Interplanetary Phenomena, Shea, M.A. and D.F. Smart (eds.), pp. 81-100. Dordrecht, Holland: D. Reidel Pub. Co., 1977.

Woo, R. and A. Ishimaru, "Remote sensing of the turbulence characteristics of a planetary atmosphere by radio occultation of a space probe," Radio Sci., vol. 8, pp. 103-108, Feb. 1973.

Woo, R. and A. Ishimaru, "Effects of turbulence in a planetary atmosphere on radio -occultation," IEEE Trans. Antennas Propagat., vol. AP-22, pp. 566-573, July 1974.

Woodman, R.F. and C. La Hoz, "Radar observations of F-region equatorial irregularities," J. Geophys. Res., vol. 81, pp. 5447-5466, Nov. 1, 1976.

Yeh, K. C., and C. Liu, "Ionospheric effects on radio communication and ranging pulses," IEEE Trans. Antemas Propagat., vol. AP-27, pp. 744-751, Nov. 1979.

Yeh, K.C. and G. W. Swenson, "F-region irregularities studies by scintillation of signals from satellites," Radio Science (Sec. D., J. of Research, National Bureau of Standards), vol. 68D, pp. 881-894, Aug. 1964.

APPENDIX 2.1
FRESNEL ZONES

To obtain expressions for the radii of the Fresnel zones, consider the two paths of Fig. A2.1. TPR is a direct path from the transmitter at T to a receiver at R, and path TSR is longer than TPR. If TSR = TPR + $\lambda/2$ where λ is wavelength, the region within the radius r of the direct path, at the distance d_T from T and d_R from R, is defined as the first Fresnel zone. Let this particular

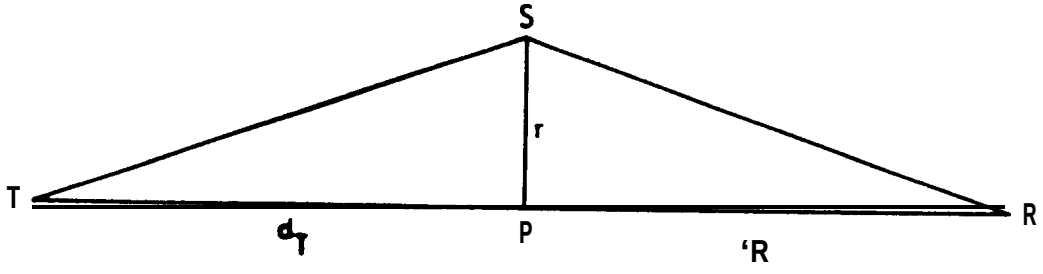

Figure AZ. 1. Geometry for consideration of Fresnel zones.

value of r be defined as F_1, the first Fresnel zone radius. Considering that the paths are such that TSP and RSP form good approximation to right triangles with $F_1 << d_T$ and $F_i <(dR$,

$$TS = \sqrt{d_T^2 + F_1^2} = d_T \left[1 + \frac{F_1^2}{2 d_T^2} \right] \qquad (A2.1)$$

and

$$SR = \sqrt{d_R^2 + F_1^2} = d_R \left| 1 + \frac{F_1^2}{2 d_R^2} \right| \qquad (A2.2)$$

Setting TPR + $\lambda/2$ = TSR gives

$$d_T + d_R + \lambda/2 = d_T + d_R + \frac{F_1^2}{2\,d_T} + \frac{F_1^2}{2\,d_R} \qquad \text{(A2.3)}$$

from which

$$\frac{F_1^2}{'T} + \frac{F_1^2}{'R} = \lambda \qquad \text{(A2.4)}$$

and

$$F_1^2 \left| \frac{'T + 'R}{'T\ 'R} \right| = \lambda \qquad \text{(A2.5)}$$

so that

$$F_1 = \sqrt{\frac{\lambda\ 'T\ 'R}{d}} \qquad \text{(A2.6)}$$

where $d = d_T + d_R$o If TSR = TPR + n $\lambda/2$, then

$$F_n = n^{1/2}\ F_1 \qquad \text{(A2.7)}$$

All the elements of radiation passing through the first Fresnel zone have components of field intensity that add constructive y. Radiation passing through the second Fresnel zone (between r = F_1 and r = F_2) interferes destructively with that passing through the first zone, and radiation passing through the third zone adds with that through the first. This condition of alternating destructive and constructive interference continues, radiation from each zone being 180 deg out of phase with that from adjacent zones, but the amplitudes of the contributions decrease with increasing n.

APPENDIX 2.2
EXPANSION OF EARTH'S MAGNETIC FIELD IN SPHERICAL HARMONICS

The Earth's magnetic field can be represented by a scalar magnetic potential as shown by Eq. (A2.8).

$$V = a \sum_{n=1}^{N} \sum_{m=0}^{n} (a/r)^{n+1} \left(g_n^m \cos m\lambda + h_n^m \sin m\lambda\right) P_n^m (\cos \theta) \qquad \text{(A2.8)}$$

The quantity is the radial spherical coordinate and a is the mean radius of the Earth (6371.2 km). The quantity λ represents east longitude measured from Greenwich, and θ is geocentric colatitude (the polar angle of spherical coordinates). The northward component of magnetic flux density Xc can be obtained from V by use of

$$X_c = \frac{1}{r} \frac{\partial V}{\partial \theta} \qquad \text{(A2.9)}$$

and the eastward component Y_c can be obtained from

$$Y_c = -\frac{i}{r \sin \theta} \frac{\partial V}{\partial \lambda} \qquad \text{(A2.10)}$$

The downward component is given by

$$Z_c = \frac{\partial V}{\partial r} \qquad \text{(A2.11)}$$

The g's and h's are the coefficients of the spherical harmonic expansion and, as mentioned on p. 2-3, these are given in the June 17,1986 issue of EOS for the 1985, fourth-generation model.